Chapter 1: Introduction

1.1 General introduction

The interdisciplinary study of biology, chemistry, and electronics is more and more important than ever before. Combining biotechnology and semiconductor technology, various types of biochips and biosensors have now been developed to detect and monitor the specific binding of biomolecules on the solid-state substrates [1]. Nowadays medical science becomes attraction, and the tools for disease diagnosis play an extremely important role. With the help of proper tools, doctors can fastly and accurately find out what's the problems with patients.

There are various biosensors such as Field effect transistor [2-3], nanowire sensor [4-7], optical sensor [8-10] etc. Planar field-effect transistor can be configured as a sensor by binding of a charged species then results in depletion or accumulation of carriers within the transistor structure [11]. The development of molecular biology and electronics, as illustrated in Figure. 1-1, increases the market of biosensors and bioelectronics. In this thesis, we fabricate a metal-semiconductor-metal photodetector (MSM-PD) as a biosensor and apply it for luminescence and gold nanoparticles detection applications. The advantage of MSM-PD device as the biosensor includes the easy fabrication and the low cost. Recent research on MSM-PD usually use III-V compound as absorption layer because electrons have lager mobility in III-V compound thus the device can operates fast and work in high frequency communication.[12-14] We use silicon substrate instead of III-V compound because a lot of III-V compounds are transparent around 450nm wavelength. Most of III-V compound materials are toxic and very expensive. Besides, the major job of absorption layer is to

transfer incident light to electrons, silicon have good absorption coefficient around 450nm wavelength.

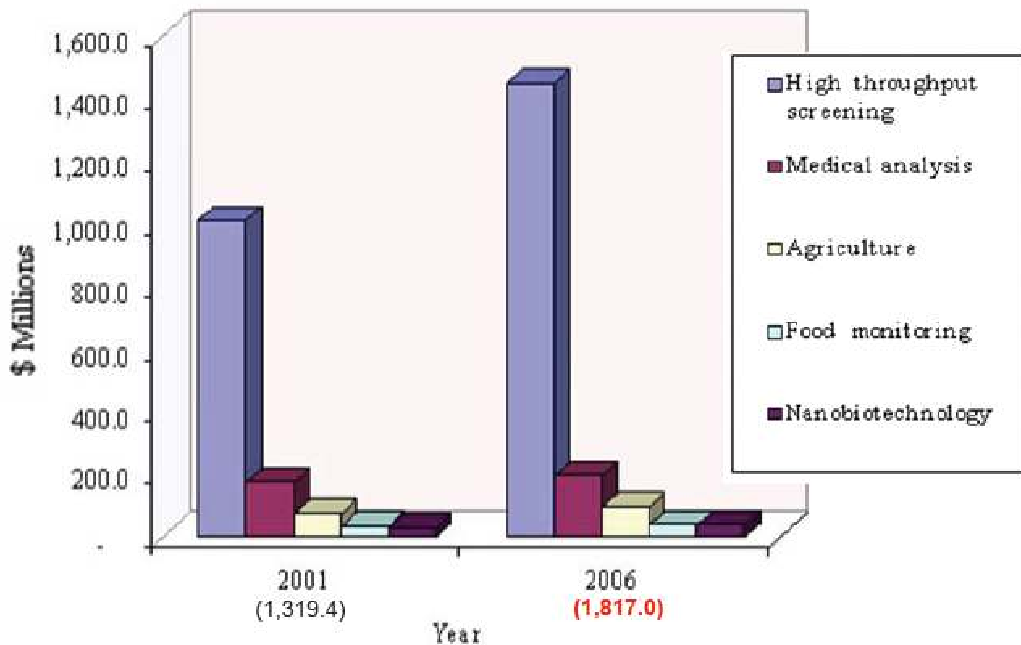

Figure 1-1. The U.S. market for biosensors and bioelectronics.

Source: BCC, Inc; http://www.bccresearch.com

1.2 Introduction of photodetector

Devices which can convert light signal to electric signal in the range of visible, infrared, or ultraviolet wavelength are known as photodetector. They are often used in systems which sense objects or encode data by a change in transmitted or reflected light. Photodetectors are classified according to their operation mechanism. One type is called photoconductive detector and the other is named photovoltaic detector [15-17]. Figure. 1-2 describe the process of collecting electron-hole pairs in photodetectors.

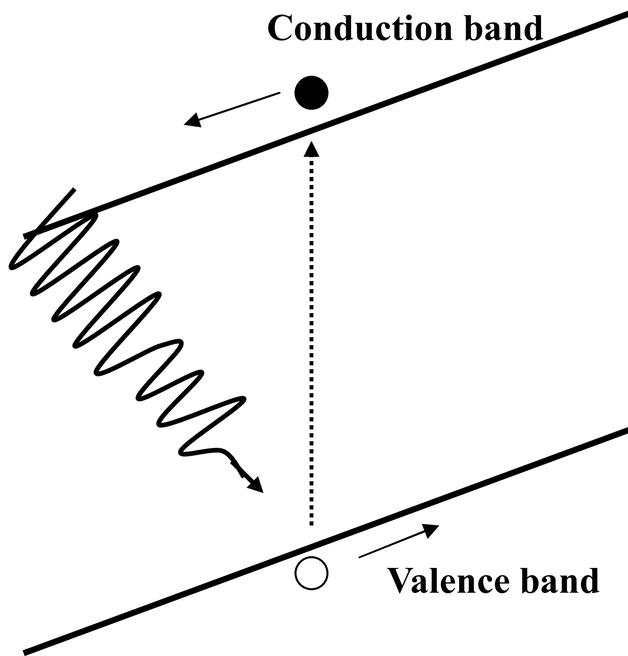

Figure 1-2. Incident light results in electron - hole pairs in semiconductor photoconduction device under bias.

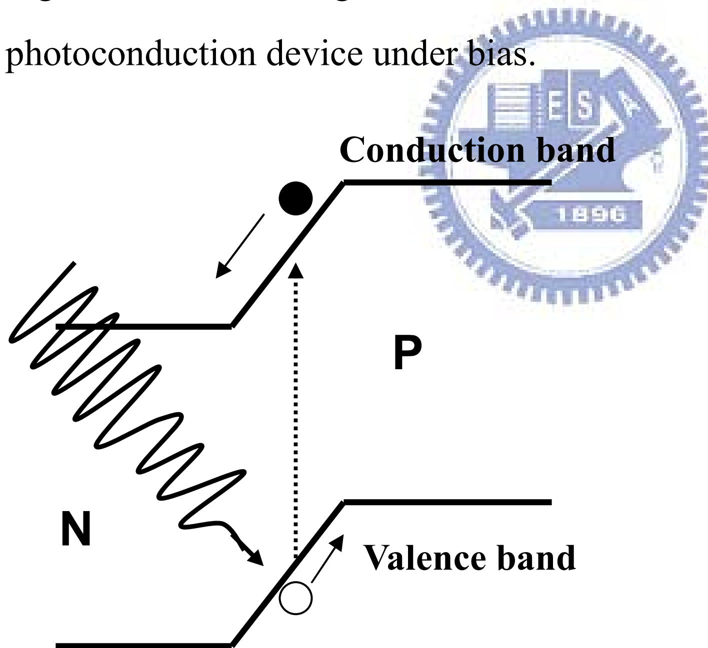

Figure 1-3. Incident light results in electron - hole pairs in semiconductor photovoltaic detector under bias.

When a photon strikes a semiconductor, it can promote an electron from the valence band to the conduction band creating an electron - hole pair. The concentration of these electron-hole pairs is dependent on the amount of light

striking the semiconductor, and therefore, the semiconductor is suitable for the optical detector. Photoconductive photodetectors detect the incident light by measuring the conductance change in semiconductors. In photovoltaic detectors such as photodiodes, a reverse-bias is applied and the light-induced electron-hole pairs determine the current through semiconductor. Photovoltaic detectors contain a p-n junction causes the electron-hole pairs to separate to produce a voltage that can be measured. Table 1 lists the specific absorbance range for various types of semiconductor materials.

Absorption layer	Wavelength(um)
Si	0.2 - 1.1
Ge	0.4 - 1.8
InAs	1.0 - 3.8
InSb	1.0 - 7.0
InSb (77K)	1.0 - 5.6
HgCdTe (77K)	1.0 -25.0

Table 1. The specific range of absorbance of light wavelength for various types of semiconductor materials.

Photovoltaic detectors such as P-N photodiode , P-I-N photodiode, and Schottky photodiode etc. have better sensitivity than photoconductive detectors However, the cost is much higher. Metal-Semiconductor-Metal photodetectors possess low cost and good sensitivity among Photovoltaic photodetector. Hence, the MSM device is a good candidate for the development of a disposable biosensor due to very low costs.

1.3 Solid-state electronic devices for biosensing

Solid state electronic devices such as nanowires [18] and nanogaps [19-20] nanoparticles [21], microcantilevers [22-23], carbon nanotubes [24-25] and quartz crystal microbalance (QCM) [26-28], are provided as the tool for the detection of protein. The advantages of them are high sensitivity and low-cost. The attachment of protein must be strong and high selective. The sensing mechanism of nanowire sensor is that when different bio-molecules binding onto the surface may affect nearby area electric field and then cause conductance changing[29]. Figure 1-4 shows that nanowire can achieve the real-time sensing for ATP molecule. Similarity, the device can detect different concentrations of target molecules.

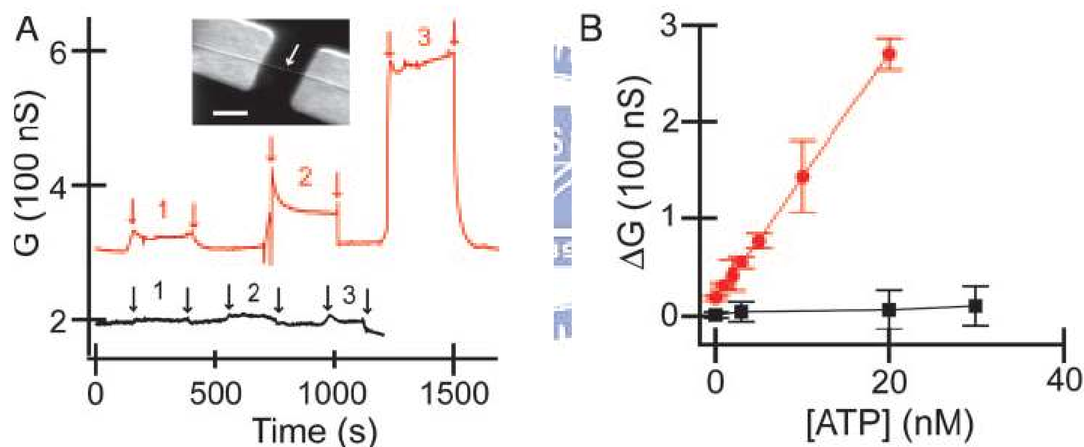

Figure 1-4. Nanowire sensor for detection of ATP binding, (a) real-time sensing, and (b) calibration curve of this device [18].

The sensing mechanism of nanogap is when the nanogap size decreasing to nanometer range, the ions between the gaps can be well-order aligned. The permittivity will change with different switching frequency, and the method is also concentration-dependent technique. Nanogap sensor had demonstrated the first time for the detection of a conformational change in protein structure.[19] The gap size is extremely important for this method and the operation has to be optimized for specific gap size as in Figure 1-5 .

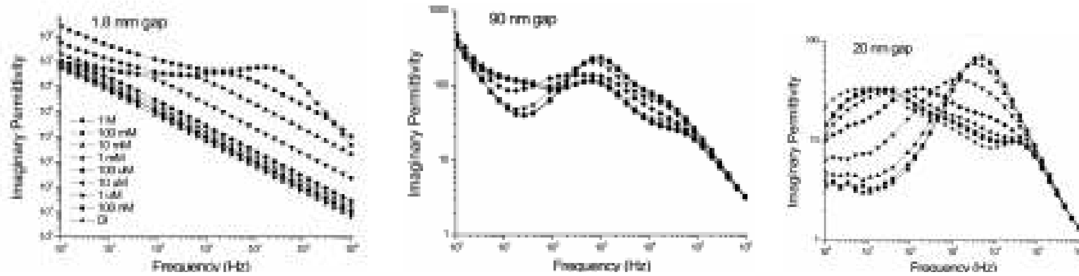

Figure 1-5 Dielectric loss data for two different nanogaps and a large commercial dielectric cell. [19]

Carbon nanotube(CNT) is the most hot topic recently. It possesses many special characteristic such as strong in mechanical strength, and it can be semiconductor, metal or insulator depending on the structure of CNT. It has been reported that protein adsorption on single-walled carbon nanotube field effect transistors (FETs) leads to appreciable changes in the electrical conductance of the devices. The phenomenon that can be exploited for label-free detection of biomolecules with a high potential for miniaturization. However, how to align CNT in specific position is still a challenge. We need to overcome this problem to obtain high yield and high stability devices.

The emission of luminescence and fluorescence in a biosystem requires the photodetectors to conver light signal into electric signal. In conventional system, the PMT is the best detector because of its high sensitivity. But recently, some small semiconductor-based photodetectors are widely studied to take the place of PMT. Figure 1-6 provides a new approach. Hybridisation probes are grafted onto the surface of the chip. After hybridization of enzyme-labelled target molecules to the probes and subsequent washes, a chemiluminescence substrate of the enzyme is added. The photons generated by the products of the enzyme-catalysed reaction are captured by the underlying photodiode, and converted into electrons.[30] The photodiode used here is charge couple device (CCD) (also called the Active Pixel Sensor, or APS) - developed essentially for

consumer camera applications (e.g. webcams, cellular phones, etc.).

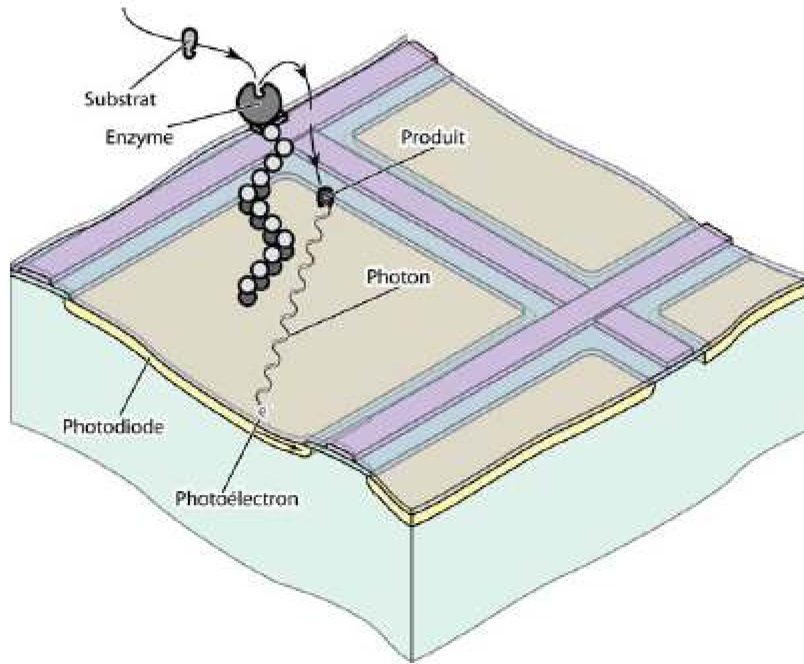

Figure 1-6. Schematic diagram of then opto-electric DNA chip at the level of 1 pixel. [30]

Researches listed above are the most modern solid state electronic device for bio-molecules detection application. They cover a wide field to integrate interdisciplinary application.

Gold nanoparticles can also be imposed on biosensor applications. P-I-N photodetectors fabricated on micromachined glass substrates are integrated with oligonucleotide-derivatized gold nanoparticles for a colorimetric detection method. The method enables the specific detection and quantification of unamplified nucleic acid sequences (DNA and RNA) without the need to functionalize the glass surface, allowing for resolution of single nucleotide differences between DNA and RNA sequences—single nucleotide polymorphism and mutation detection. The detector's substrate is glass and the sample is directly applied on the back side of the biosensor, ensuring a direct optical coupling of the assays with a concomitant maximum photon capture and

the possibility to reuse the sensor.[31]

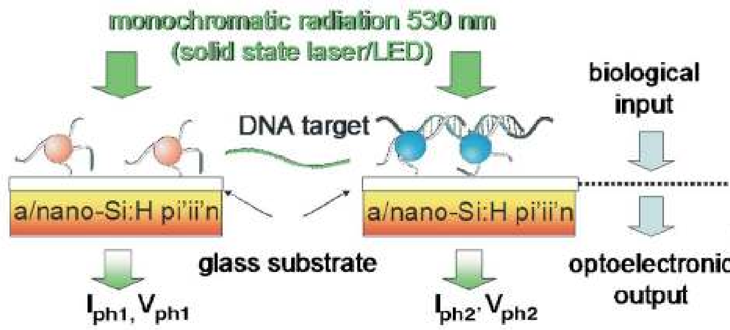

Figure 1-7. Schematic diagram of detection platform used in literature. [31]

1.4 Motivation

Nowadays nanotechnology is wildly researched in all subjects because of its versatility. In semiconductor industry, the rapidly progressive revolution leaves huge impression on me. The feature size of device is smaller and smaller, as we know that the smallest commercial product on the market is 65nm. Miniaturized devices have lots of advantages such as power saving, high sensitivity, high operation speed, and portable.

Since the first developments in the late 1980s, DNA hybridization chips have evolved into a powerful tool providing complex informative data from nucleic acid sequences. Taking advantage of the acceleration of genomics discoveries, this technology has proven invaluable in many fields of research and diagnostics. The use of quartz crystal microbalances (QCM) monitor the mass and viscosity changes that occur upon hybridisation of targets on probes grafted onto the surface of the crystal.

By combining semiconductor technology and self-assembly techniques I want to provide a new approach in detecting DNA or Protein of enzyme-catalyzed luminescence MSM-PD biosensor. Our ultimate goal is to develop a cheap and portable devices which possessing high sensitivity.

By means of enzymes that catalyzes a chemiluminescence reaction, light generated on the reaction chamber is measured by the underlying MSM-PD. The output of the system can be quantitatively from the signal generated by above detector. This simple and robust system shows surprisingly high sensitivity with only a simple electric interface to the recording system. It thus fulfils the requirements for integration of electric detection methods in the disposable micro-devices designed for decentralised diagnostics tests.

Chapter 2: Device principles and operations

2.1 Fundamentals of the MSM-PD

The MSM-PD is a planar device, and it consists of two back-to-back connected Schottky diodes on a semiconductor layer. The metal structure is composed of two contact pads and interdigitated lines, which form the active area of the device. The device works by absorbing optical energy and converting incident photons into a time-varying electrical signal. When the active area of the device is illuminated, carriers in the semiconductor absorption layer (also known as electron-hole pairs) are generated by incident photons having energy greater than the bandgap energy (E_g). The carriers are transported to the metal contact pads, and a current is detected in the external circuit under the application of an external bias voltage. Figure 2-1 shows the cross section of the MSM-PD, signifying the dimensions, carrier motion, and the electric field orientation. S and W refer to the electrode spacing and width, respectively, d to the thickness of the active area, and E to the electric field.

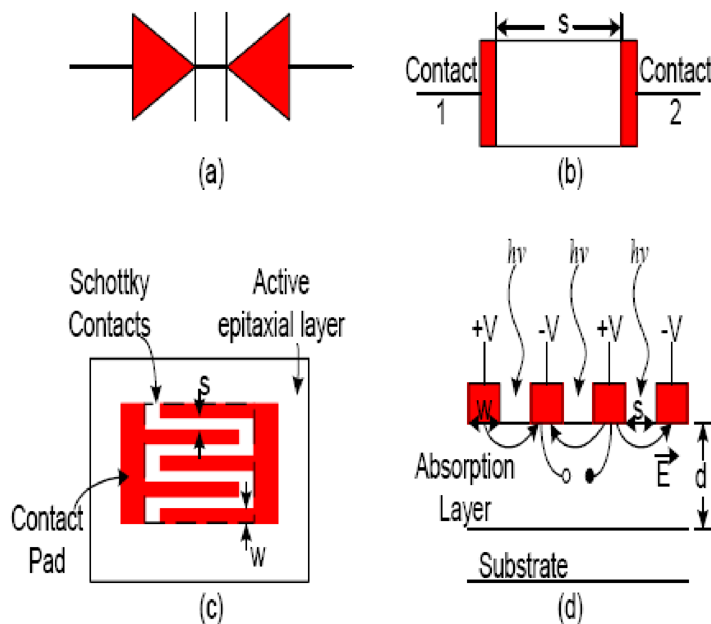

Figure 2-1. (a) schematic symbol, (b) 1-D schematic, (c) top view, and (d)

cross-sectional view.

2.2 Semiconductor physics of the MSM-PD

2.2.1 Schottky diode

A Schottky diode, also known as metal-semiconductor photodiode is formed when a thin semitransparent metallic film is brought into contact with a semiconductor to form a metal-semiconductor junction. Under the Schottky-Mott theory [1], a potential barrier arises due to the difference in work functions of the metal and semiconductor. If the work function of the metal is greater than that of the n-type semiconductor ($\phi_m > \phi_s$), the electrons in the semiconductor will transfer from the semiconductor to the metal until the Fermi levels are equal. On the contrary, the work function of the metal is lower than that of p-type semiconductor ($\phi_m < \phi_s$). The electrons in the metal will transfer from metal to semiconductor until the Fermi levels are equal. The equilibrium energy band diagram of Schottky barrier junctions in both cases are shown in Figure 2-2, where ϕ_m is metal work function, ϕ_s is semiconductor work function, χ_s is the semiconductor electron affinity, ϕ_b is the Schottky barrier height, V_{bi} is built-in voltage, which equals to $\phi_m - \phi_s$. The Schottky barrier height for both n-type and p-type cases are given, respectively

$$\phi_{Bn} = \phi_m - \chi_s \quad (1)$$

$$\phi_{Bp} = E_g + \chi_s - \phi_m \quad (2)$$

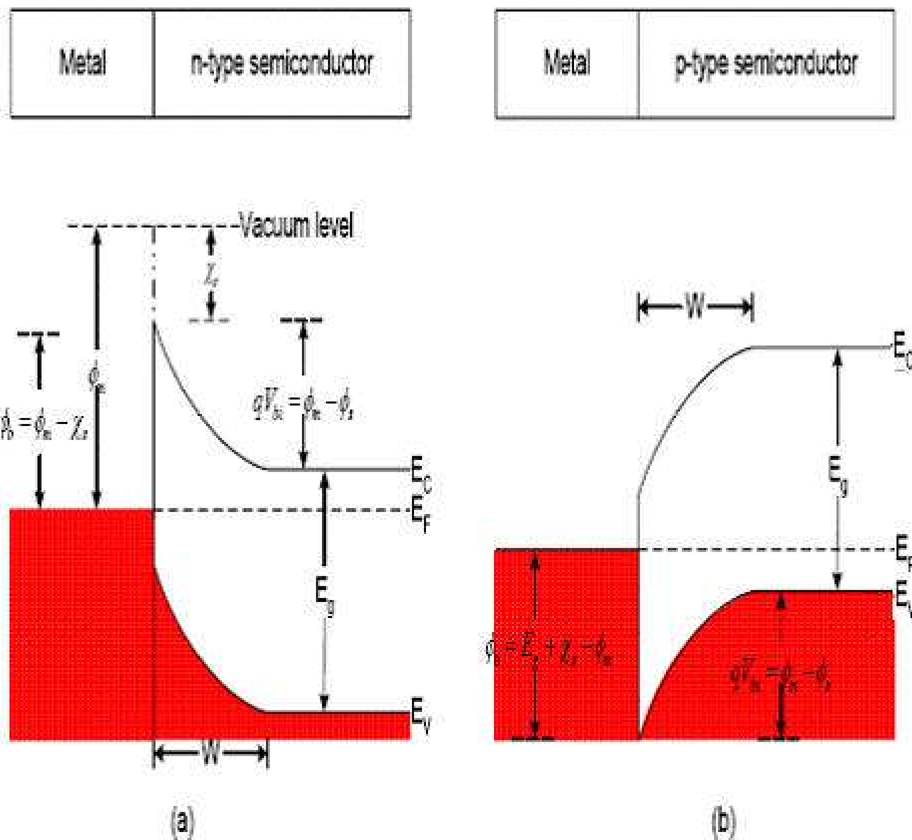

Figure 2-2. Schottky diode under thermal equilibrium condition, (a) metal and n-type semiconductor($\phi_m > \phi_s$), (b) metal and p-type semiconductor($\phi_m < \phi_s$).

Figure 2-3 (a) illustrates a schematic diagram of symmetrical MSM structure with metal contacts to uniform-doping n-type semiconductor. The charge distribution, electric-field distribution, and energy-band diagrams in this device with a small positive bias voltage are shown in Figure 2-3 (b), (c), (d), respectively [2-4]. As a small positive bias voltage is applied, one side is forward-biased and the other one is reverse-biased. The W_1 and W_2 denote the depletion widths at the forward and reverse bias Schottky junctions in the n-type semiconductor, respectively.

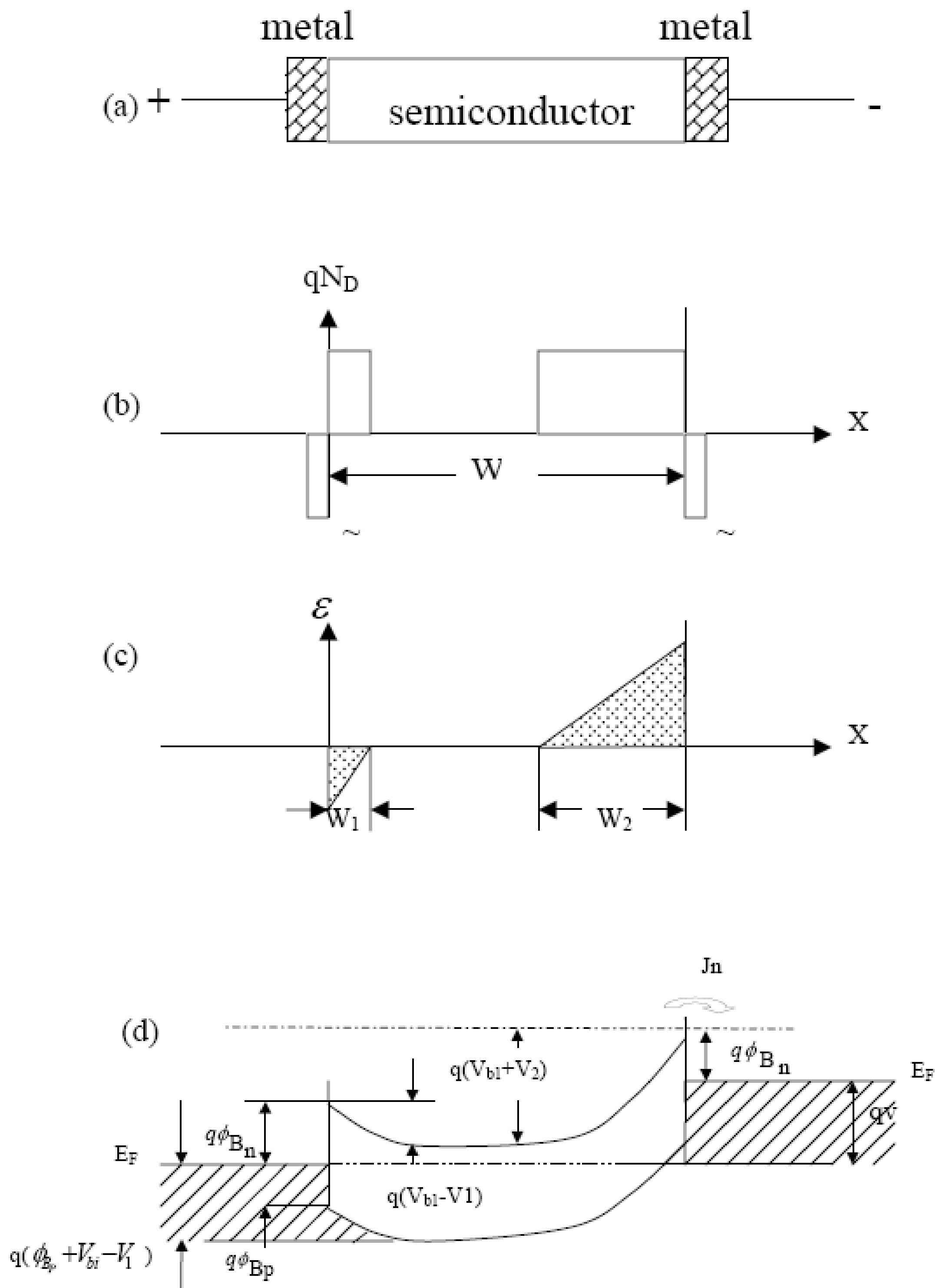

Figure 2-3. (a) schematic diagram of MSM-PD, (b) charge distribution under low bias voltage, (c) electric field distribution under low bias voltage, (d) energy band diagram of MSM-PD.

2.2.2 Current Transport Mechanism

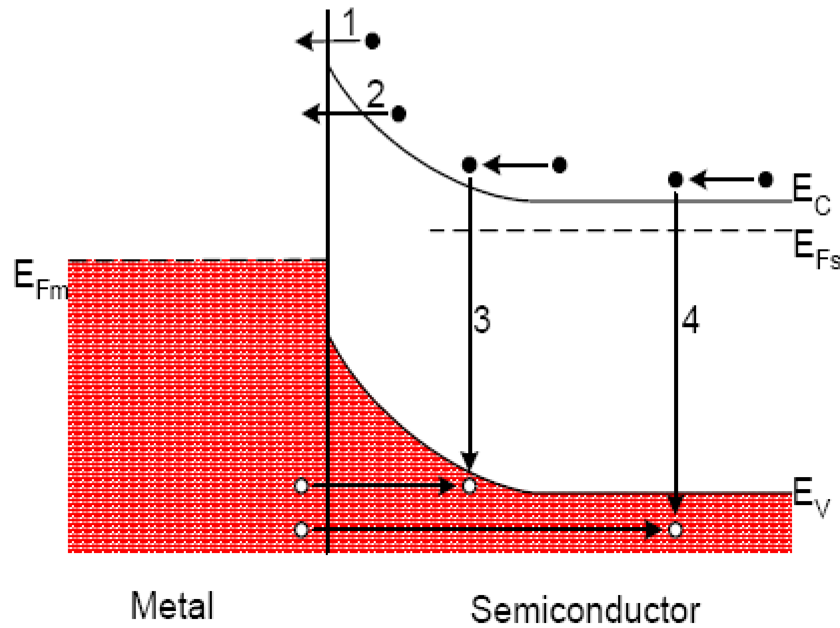

Figure 2-4. Current transport mechanism under forward bias.

The current transport in metal-semiconductor contacts is primarily due to majority carriers. The four basic transport processes for a Schottky diode[5-7] are shown in Figure 2-4 under forward bias conditions (the inverse processes occur under reverse bias):

(1) Emission of electrons from the semiconductor over the top of the potential barrier into the metal

(2) Quantum mechanical tunneling of electrons through the barrier

(3) Recombination in the space-charge region

(4) Recombination in the neutral region (also hole injection from the metal to the semiconductor)

Condition (1) and (2) are dominant for moderately doped semiconductor, and heavily doped semiconductors, respectively. Diffusion[8-9], thermionic emission[10], and combined thermionic emission diffusion[11-12] theories are

used to study the emission of electrons over the barrier. The thermionic emission theory applicable to high-mobility semiconductors; and for low mobility semiconductors the transport is described by the diffusion theory.

2.3 Characteristic parameters of MSM-PD

2.3.1 Quantum efficiency

Quantum efficiency, η $(0 \leq \eta \leq 1)$ of a photodetector is defined as the number of carriers (electron-hole pairs) collected to produce the photo current (I_{ph}) generated per the number of incident photons(P_{in}). The equation of external quantum efficiency (η) is given by

$$\eta = \frac{I_{ph}/q}{P_{in}/h\nu}$$

Where q is magnitude of the electronic charge, h is Plank constant, ν is the frequency of incident light.

2.3.2 Responsivity

Responsivity of the detector is the ratio of the photo current flowing in the detector to the incident optical power:

$$R = \frac{I_{ph}}{P_{in}} = \frac{\eta\lambda}{1.24} \quad (A/W)$$

Where λ is the wavelength of incident light.

2.3.3 Response time

The response-time limit of all photodetectors is determined by basically

three effects: the time of carrier diffusion to the junction depletion region, τ_0; the transit time of carrier drift across the depletion region, τ_s; and the RC time constant associated with circuit parameters including the junction capacitance C and the parallel combination of device resistance and external load.

Chapter 3: Experiments

Single-crystalline N^+-type <1 0 0> silicon wafers with resistance 2-7(Ω-cm) were used through all the experiments.

3.1 Device fabrication techniques

The details processes of Metal-Semiconductor-Metal photodetector (MSM-PD) are listed below.

3.1.1 Fabrication process

Step 1: Standard clean [1] is applied to the silicon wafer. Firstly using the DHF to remove the native oxide on the silicon surface, secondly rinsing the wafers in NaOH (SC-1) removes particles and some organic compounds, then rinsing the wafers in HCl (SC-2) removes alkaline metallic ions and alkaline-earth metallic ions. Since H_2O_2 was added in SC-1 and SC-2 to improve the activity of the chemical, the oxidative activation of H_2O_2 will result in native oxide. Finally rinsing the wafers in DHF to remove the native oxide to ensure the silicon surface is situated on the top of the surface.

Step 2: Put the wafers into Low pressure furnace tube to grow thermal oxide 2000 Å.

Step 3: Spin coating E-beam positive photoresist on the wafers.

Step 4: Using E-beam lithography (Leica WetPrint 200) to write the zero mask pattern on the wafers. (The zero-mask is for alignment calibration.) Afterward develop the wafers in TRACK (TEL CLEAN TRACK MK-8). 2.38% Tetramethyl ammonium hydroxide (TMAH) solutions was used for

development.

Step 5: Etching the oxide layer by reactive-ion-etching (RIE)[2] (TEL5000).

Step 6: Remove the photoresist by OZONE plasma (FUSION OZONE ASHER) and then rinse in SPM solution (H_2SO_4 : H_2O_2 = 3 : 1, 120^oC). Then rise in SC-1 to remove side-wall polymers formed during step 5.

Step 7: Etch the silicon layer by TCP. Zero mask patterns are finished here.

Step 8: Depositing thermal oxide (DRY OX) 350Å by Low pressure horizontal furnace tube.

Step 9: Spin coating positive E-beam photoresist, afterward pattern the active window by E-beam lithography. Then Develop by TRACK.

Step 11: Etching dry oxide layer by TEL5000. Then rinse in SC-1 to remove side-wall polymer.

Step 12: Remove photoresist by OZONE and SPM.

Step 13: Spin coating photoresist and then pattern interdigitated lines by E-beam lithography. Develop by TRACK.

Step 14: Using TCP to etch the single crystalline silicon to make sure the metal lines have good adhesion and contacts with the silicon surface.

Step 15: Depositing metals by thermal coater (Cr, Au) or Electron-Gun(Cr, Pt).

Step 16: Using lift-off techniques to remove the unwanted metal.

Step 17: Depositing oxide passivation layer by PECVD. The thickness is 760Å.

Step 18: Spin coating E-beam positive photoresist then E-beam lithography to make the pattern of probe contacts. Then develop by TRACK and etch by BOE (Buffered oxide etching solution NH_4F: HF = 5:1) The device is completely finish here.

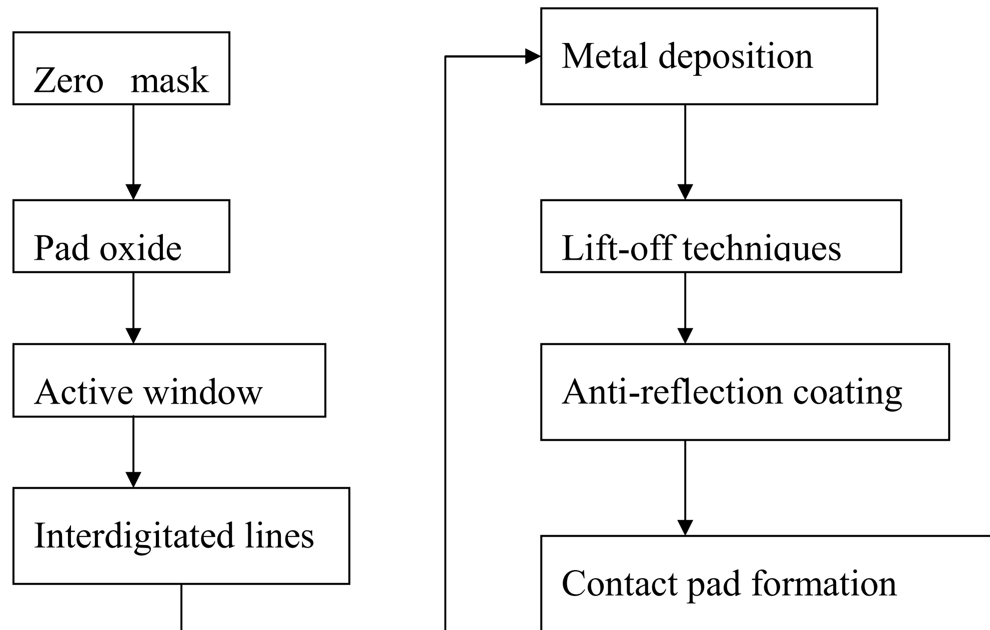

Figure 3-1. Process flow chart of MSM-PD fabrication.

3.1.2 E-beam lithography

The common lithography techniques in semiconductor manufacturing technology are G-line, I-line, and E-beam lithography, etc. The G-line lithography has critical size 436nm, and I-line is 365nm. The critical size of pattern is 300nm and the density of pattern is extremely high, thus G-line and I-line can't satisfy our requirements. Consequently, we choose E-beam lithography to accomplish the patterning realization. Electron beam lithography is able to provide high resolution patterning down to nanometer scale.

3.1.2.1 Ideas for device layout

I will describe the layout of MSM-PD is illustrated here. The MSM-PD is designed for detecting luminescent light, and luminescent reaction is in liquid state. We need to design a reaction chamber which can isolate the liquid solution to avoid the problem of short circuit. The diameter of the reaction chamber is

5mm excluding the thickness of the chamber wall, thus plus the thickness of the chamber wall the total diameter is about 7~8 mm. The distance between two contact pads of the MSM-PD is 8mm. The contact pad is 1000um*1000um square for easy electrical probing consideration. The line width is 300nm and the space is 300nm (as shown in Figure 3-2(b)). The active region is 100um*100um containing 83 lines in each side. The active region layout of MSM-PD is in Figure 3-2(b) is the trim version.

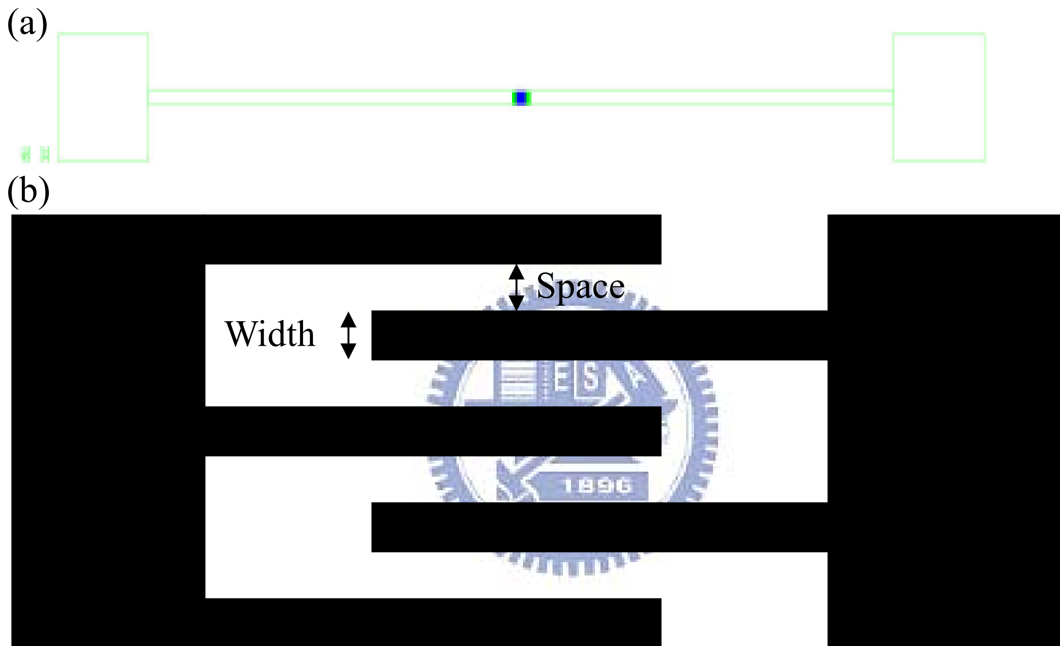

Figure 3-2. (a) Full layout of MSM-PD, the dark area in the middle is the active area, the two squares in both side is contact pad, (b) Magnification image of active region, the active area contains 83 lines per side.

3.1.2.2 Introduction of proximity effect

When an electron beam is incident on a photoresist, the electrons are not destroyed but are scattered both elastically (without momentum energy loss) and inelastically (with momentum energy loss). The elastically scattered electrons generally have sufficient energy to travel a long way. Those which head back

toward the source are called the back-scattered electrons. The inelastically scattered electrons generate additional radiation quanta through their energy loss, including X-rays, Auger electrons, and low-energy ejected electrons (also called secondary electrons)[3-6]. The range of the back-scattered electrons is much larger than the range of the secondary or Auger electrons due to their higher energy. Back-scattered electrons in dense pattern area often cause critical size to be wider than the design pattern. Most electron-beam lithography systems compensate for this pattern dependence by reducing the dose in densely patterned areas than in isolated features. The advantage of electron beam lithography machines is their ability to produce small critical sizes. But as critical sizes decrease, the proximity effect becomes more and more important. The proximity effect limits the resolution of electron beam lithography. Therefore, the proximity effect correction is required to minimize the pattern deviation.

3.1.2.3 E-beam proximity effect correction method

Here we will discuss the strategy to solve the problem of proximity effect. The most important parameter in E beam machine is to find the dosage (the amounts of electrons hitting on resist).

Electron beam dose formula: ED Factor*resist*1/100 (μC/cm^2).

resist=100 ; Current density=4.0 (A/cm*cm) ; ED (E-beam dosage) Factor is the parameter we have to test to find the best dosage. I try dose 3~10(μC/cm^2) and the step is 0.2(μC/cm^2).

The interdigitated lines are highly concentrated and the line width to space ratio is 1:1. We encounter proximity problems and need to be solved. Figure 3-3 is the

In-line SEM of interdigitated lines without any correction method. We can see that in the upper part in Figure 3-3, in the densely region (width to space= 1: 1) the photoresist are overexposed. The patterns of interdigitated lines are all collapsed.

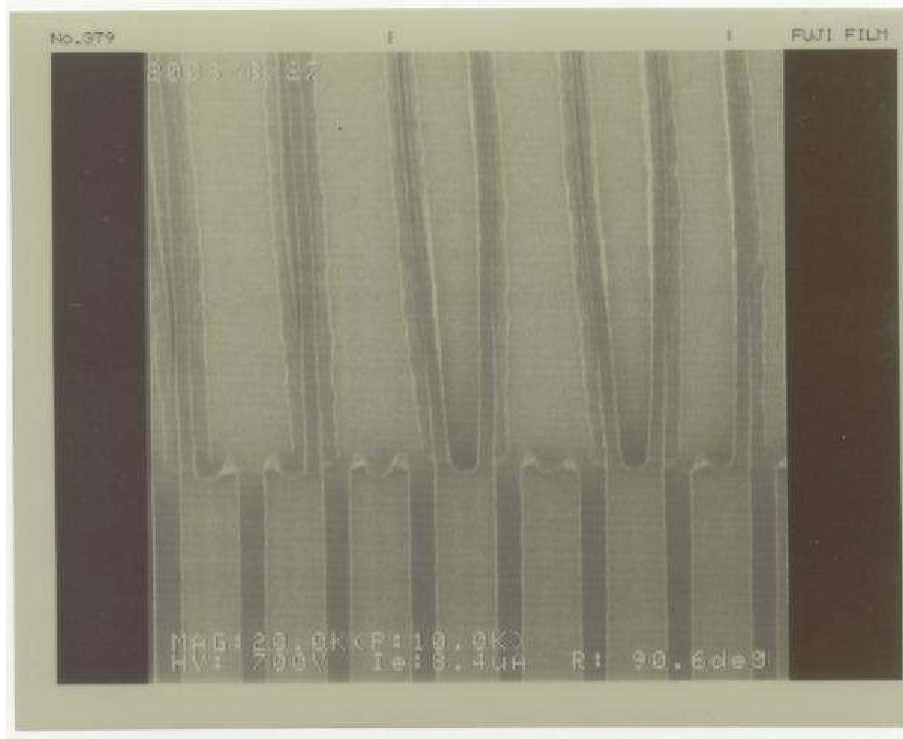

Figure 3-3. In-line SEM image of interdigitated lines by E-beam lithography but without any correction method (dark color is silicon; white color is resist).

Firstly we try E-beam proximity correction (EPC) method. The method is based on the characteristics of photoresist type, and with the help of computer simulation to modify pattern layout. It will change the segments of our layout pattern to compensate the back scattering electrons which will cause over-exposure to the resist. The name of this software is PROXECCO and it is designed for arbitrary structures and very complex circuits. It combines high pattern fidelity with very efficient and extremely fast methods for calculation. The exact preservation of the pattern geometry is a main feature of this tool. The

accuracy and efficiency of PROXECCO are based on a separate treatment of pattern and correction. The mathematical algorithm uses an improved version of the deconvolution method. The development pattern is determined by the energy distribution in the resist, and the simulation shows an energy distribution in the resist. We can observe that there are regions with higher deposited energy in the middle and lower energy in the border. This inequality is responsible for the proximity effect. The deposited energy can be described as the applied dosage convoluted with the proximity function. Thus the problem of describing proximity effects is reduced to describing the proximity function. The proximity function depends on almost everything in the lithography system: beam energy, resist type, substrate etc. A common approximation is the double Gaussian model: The proximity function is represented by a sum of two Gaussian functions. There are three relevant parameters for such an approximation: α describes the width of the narrow peak coming from the forward scattered electrons, β describes the width of the broad underground which is the contribution of the backward scattered electrons, and ζ stands for the relation between the content of the two Gaussian functions. A typical value for ζ is approximately 1.0. This means the direct and neighborhood exposure can be of the same quantity. In a large plane only half of the exposure is then coming from the direct beam, and the other half comes from the neighborhood. Figure 3-4 is the result after EPC, the pattern can be completed well, although the outer areas are not perfectly patterned. There is still some photoresist covering underlying silicon in the underexposed area, in the succeeding step (metal deposition) these lines will be broken and can not provide current path. But this drawback is

acceptable, don't forget we have 83 lines per side. The main point we concerned with is that the metal lines can't cross touch with each other, it will cause short circuit and the device is dead then. Figure 3-5 shows the line width is 293nm, which is very close to 300nm.

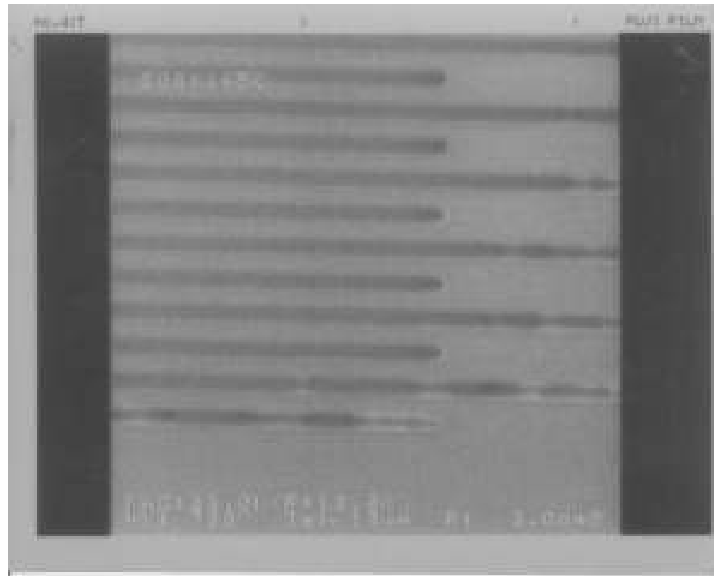

Figure 3-4. In-line SEM image of interdigitated lines after EPC modification. The right-down areas are not exposed perfectly duo to underexposed. (dark color is silicon; white color is resist)

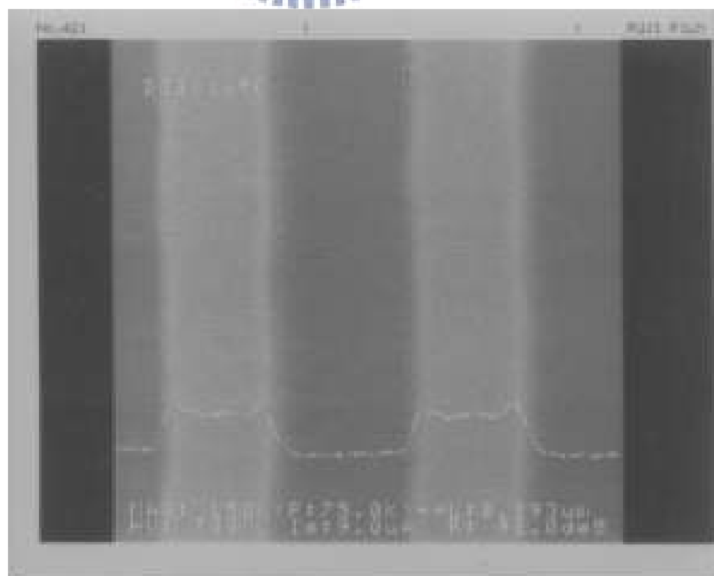

Figure 3-5. The In-line SEM image shows the resist width of 293nm. (dark color is silicon; white color is resist)

We acquire some experiences from EPC method after a series of works. We separate the semi-dense (width to space is 1:3) and dense areas (width to space is 1:1) in different layers, and apply different electron beam dosages in semi-dense and dense area. The origin line width is 300nm and space is 300nm, and in the new layout the line width is 250nm and space is 350nm. The reason is that electrons may scatter from neighborhoods making line width wider, thus we decrease the line width to compensate the neighborhoods scattering electrons.

It works out perfectly by this method. Figure 3-6 shows the perfect pattern after development and is measured by in In-line SEM, and Figure 3-7 shows the line width is close to the designed 300nm.

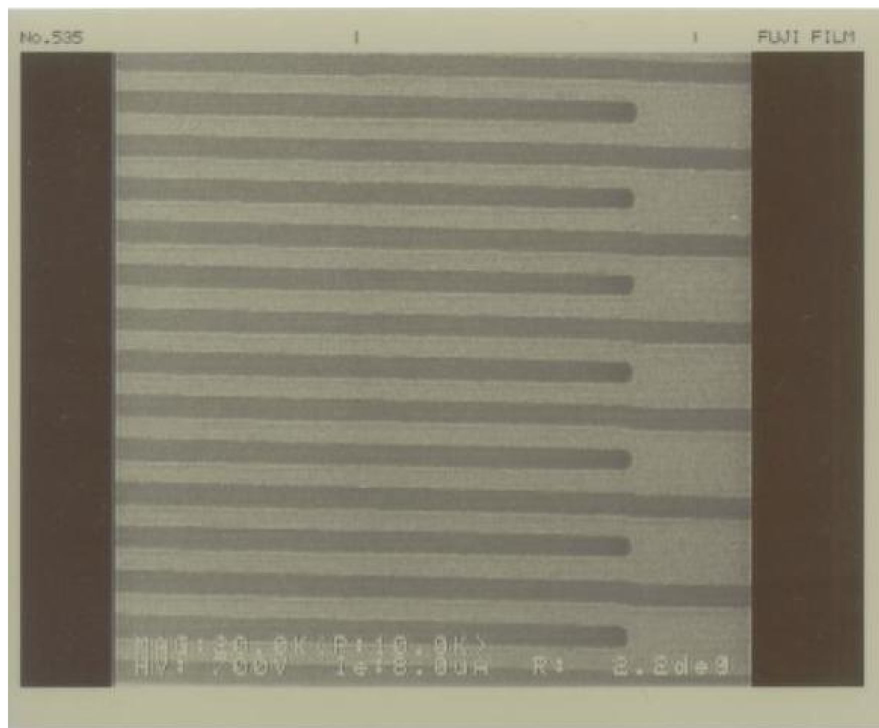

Figure 3-6. In-line SEM image of interdigitated lines, this correction method is by manually decreasing the line width of the layout. (dark color is silicon; white color is resist)

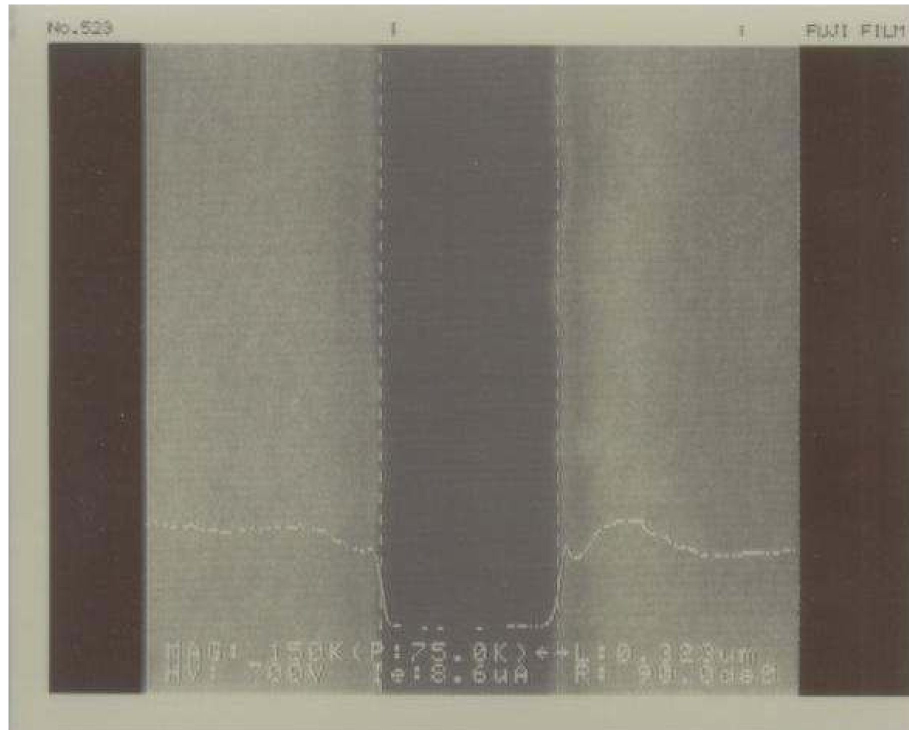

Figure 3-7. The line width is 323nm from In-line SEM measurement. (dark color is silicon; white color is resist)

3.1.3 Lift-off process

3.1.3.1 Introduction of lift-off process

"Lift-off"[7-10] is a simple, easy method for patterning films that are deposited onto a pre-patterned photoresist layer. It omits a couple of processing steps. Firstly a pattern is defined on a substrate via lithography on photoresist. A film, usually metallic, is deposited all over the substrate covering the photoresist. In areas which the photoresist has been developed the metals contact directly with underlayer. When soaking the wafer in solutions that can dissolve photoresist, metals on the top of photoresist will be removed. On the contrary, only metals contact directly with layer which is under photoresist can be preserved.

In semiconductor fabrication process, the lift-off techniques usually uses to

patterned metal lines because dry etching techniques can't etch many metallic films, such as gold, platinum, etc. Furthermore, lift-off techniques can't only apply to pattern metallic films but also some insulator or dielectric materials, it plays an important role in semiconductor fabrication because of its versatility. The lift-off process is illustrated in Figure 3-8.

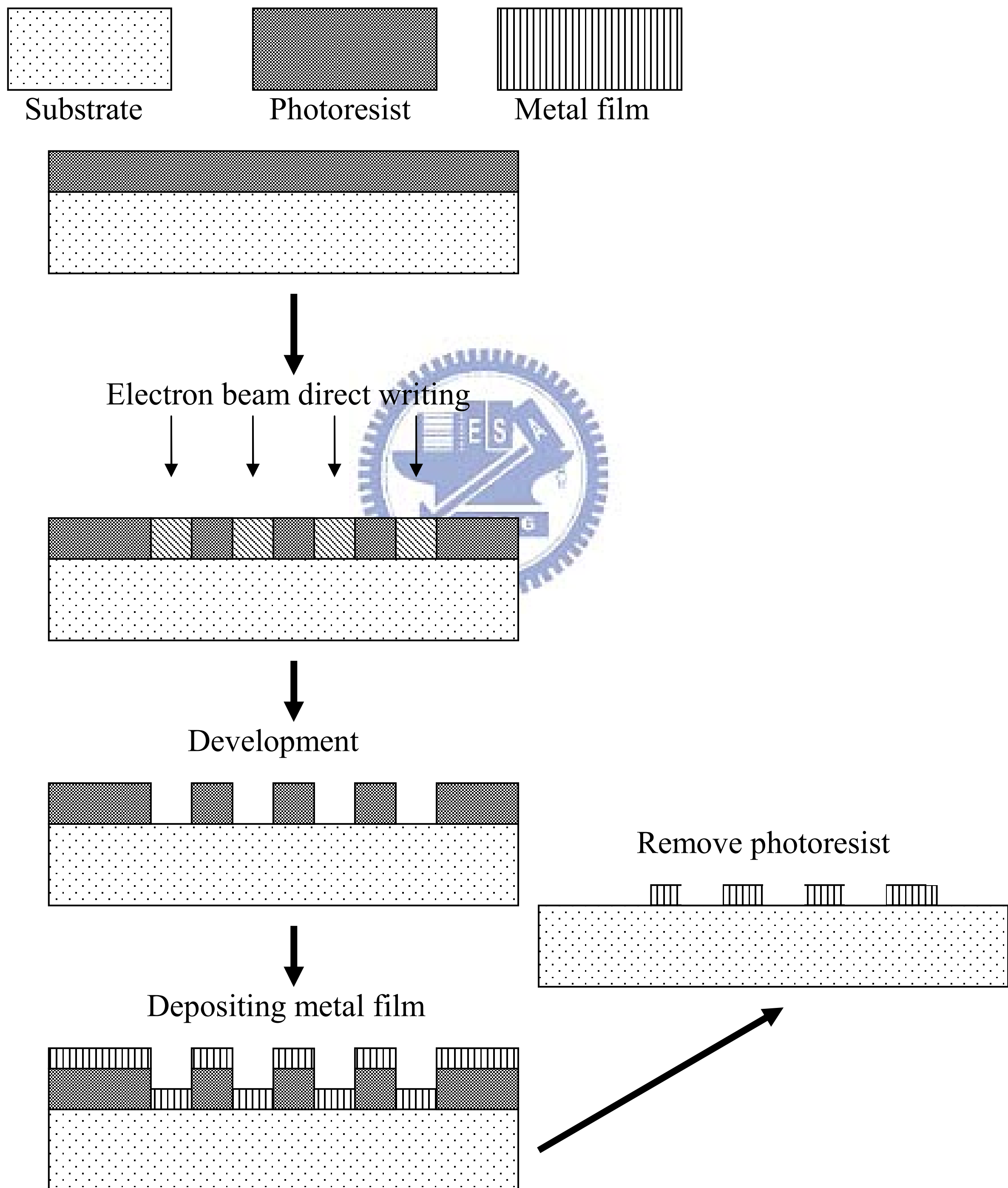

Figure 3-8. Lift-off process flow chart.

3.1.3.2 The problems during lift-off

The removal of photoreisit taking away unwanted metals is the key point in lift-off techniques, success or not depends on this step. Different types of photoresist have its specific etching solutions. We have tried three kinds of solutions including NMP (1-Methyl-2-pyrrolidone; C_5H_9NO), acetone, SPM (H2SO4:H2O2=3:1) in order to find the best solutions in loft-off process.

Firstly we study etching solution of NMP, after soaking the wafer in the solution for 4 days and then check the patterns by optic microscopy. The results show no significant changes in pattern formation, i.e. the photoresist didn't dissolution in the etching solution (maybe the solution not contact with photoresist yet), and the unwanted metals had still not been removed. Secondly we try soaking the chip in acetone. But the results indicate that acetone is even worse comparing with etching solution of NMP. Figure 3-9 is the optical microscopic image after four days rinsing in etching solution. We can see the unwanted metals still remain on the active area.

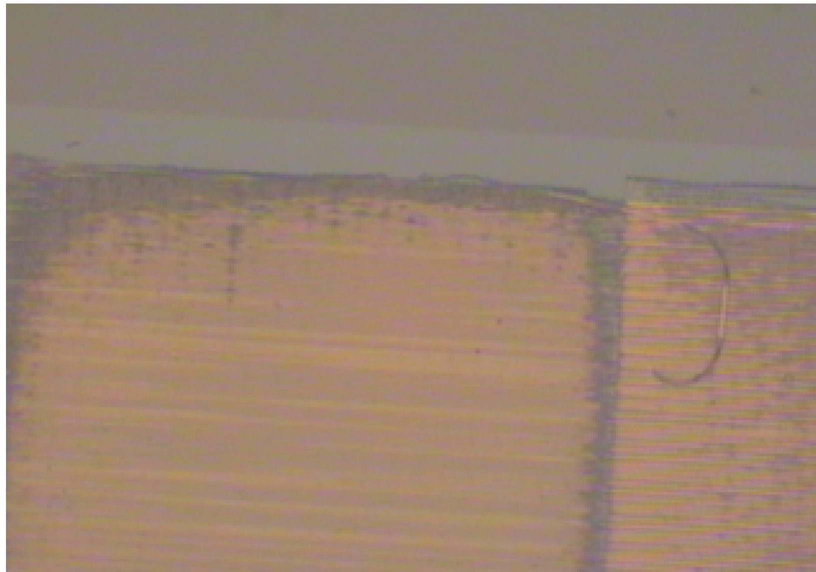

Figure 3-9. Optical microscopic image of interdigitated lines: soaking in etching solution of NMP for 4 days.

Finally I try soaking the chip in SPM for 1 hour, the SEM image shows the patterns are terribly damaged. The metals are not only falling off but also becoming fragmented lines in Figure 3-10, 3-11.

The SEM analysis of interdigitated lines after conventional lift-off process by SPM is listed in Figure 3-10, 3-11, the line width is 300nm, and the space is 300nm. Due to the small contact areas between metal and silicon substrate, the adhesion force is not enough to against the upper force. It will result in fragmented lines and it will cause an open circuit, while cross touching metals will cause short circuit.

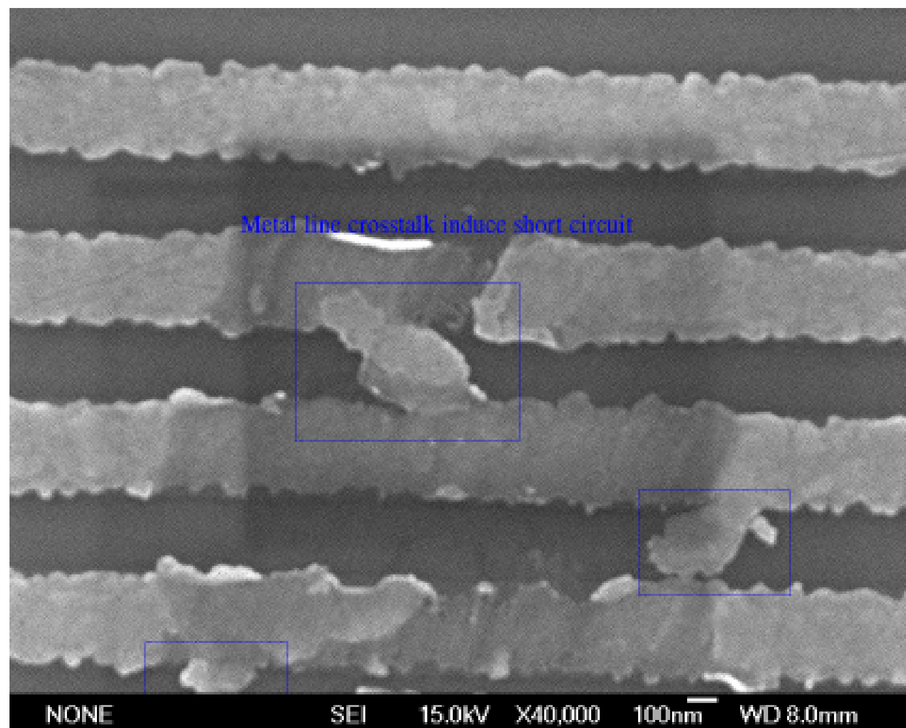

Figure 3-10. The SEM image of interdigitated lines. (cross-touching leading to short circuit; width: space = 1:1)

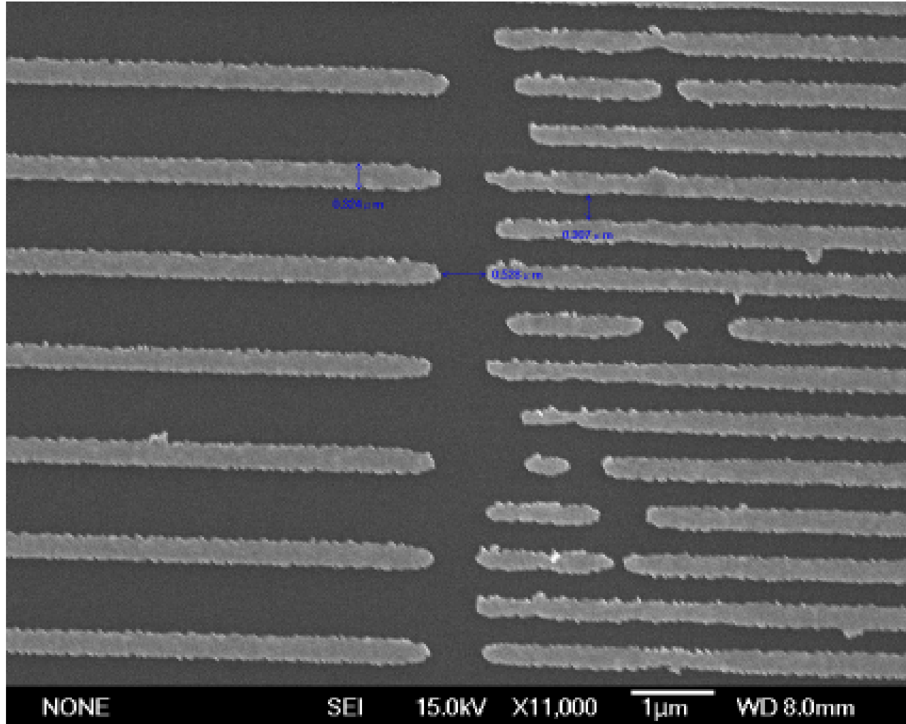

Figure 3-11. The SEM image of adjacent region between semi-dense area (width : space = 1:3) and dense area (width : space= 1:1); (fragmented lines leading to open circuit).

3.1.3.3 Solutions for these problems

In this section, we will describe how to solve this problem. We begin with the problems of pattern structure leading to lack of adhesion force between metal and silicon. And then by try-and-error I summarize the best procedure for lift-off process.

In order to overcome this drawback in Figure 3-10, 3-11, we add a process before depositing metals (see Figure 3-12). By etching down the crystalline silicon of substrate by TCP, it can provide more contact areas between metal and silicon thus resulting in better adhesion force.

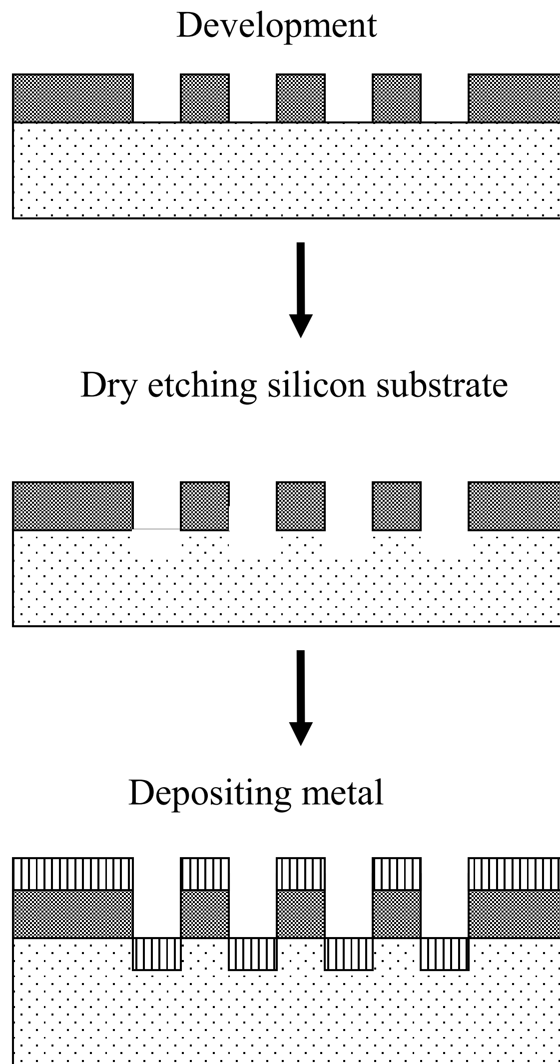

Figure 3-12. New process flow chart of lift-off by etching down unerlayer.

Figure 3-13 shows the SEM analysis after solving structure problem. Compare with Figure 3-10, 3-11, the fragmented lines no longer exist, and the patterns are much better now.

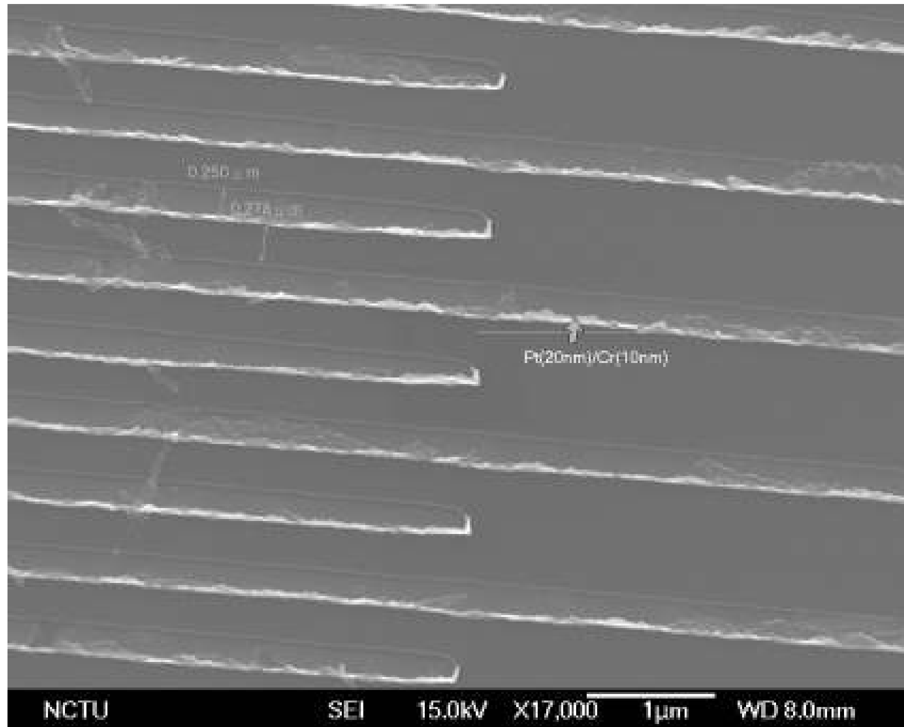

Figure 3-13. The SEM image of adjacent region between semi-dense areas (width : space = 1:3) and dense areas (width : space= 1:1) by means of improvement method.

After lots of tests by try-and-error, I summarize the best lift-off process as below:

Step 1. Rinse the photoresist in etching solutions of NMP for 4 days, and then wash by DI water and nitrogen purge.

Step 2. Rinse in SPM for 10 minutes

Step 3. Put in DI water and then use sonication for 3 seconds. Followed by nitrogen purge.

Since rinsing chip in etching solutions for 4 days doesn’t take effect for removing unwanted metals. From previous tests we know the reaction between SPM and photoresist is very violent, thus it can rapidly remove photoresist. We dip the wafer in SPM at 120^0C for 10 minutes. Figure 3-14 shows the patterns

after soaking in SPM. The residues of unwanted metals may be sticky with surrounding metals. Thus we employ sonication to remove residual metals. As we can see in Figure 3-15, the final pattern is completely finished.

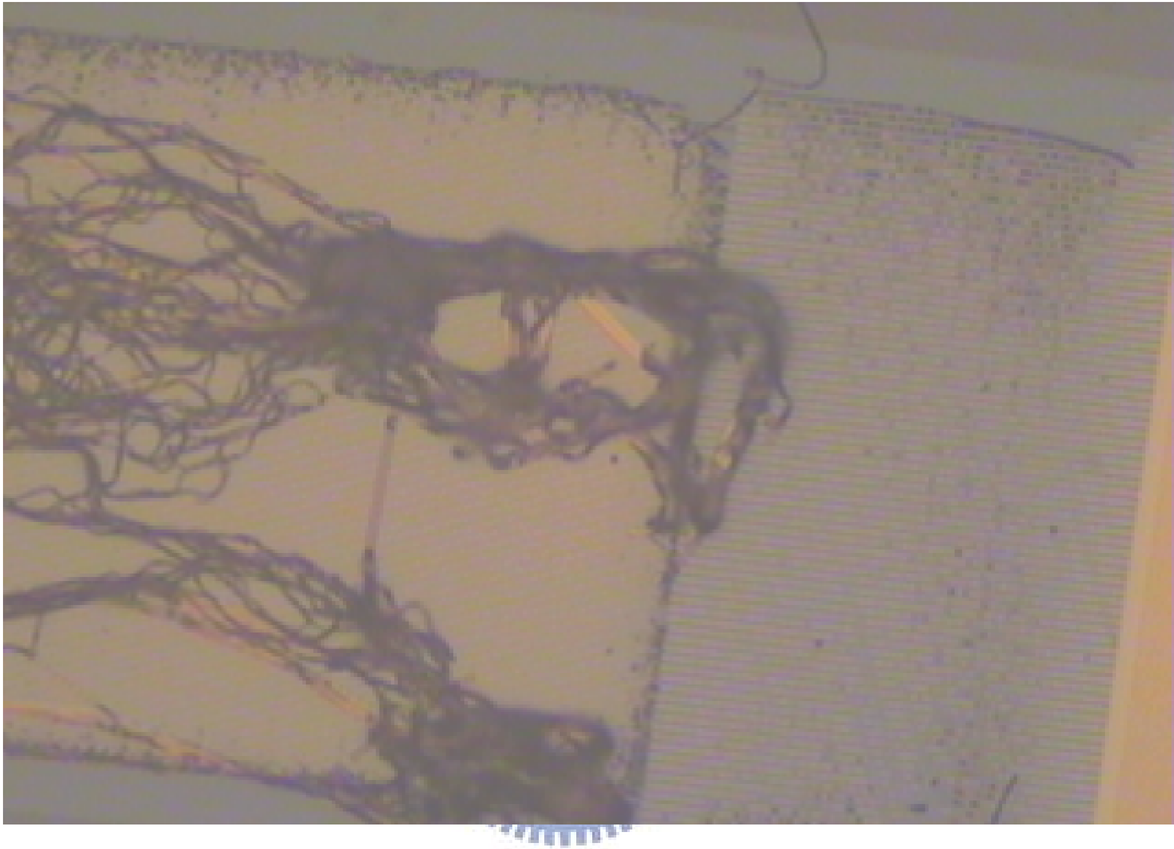

Figure 3-14. Rinsing in etching solutions for 4 days and then rinsing in SPM for 1 hour.

The sonocation time is extremely important in step 3. If the time of sonication is too long, the metal lines can not against the upper force leading to lose metal lines. Figure 3-16 shows that lots metal lines missing after 6 second sonication. Readers must pay attention to the step during lift-off .

Figure 3-15. Optical microscopic image of interdigitated lines. Condition: Figure 3-14 after performing sonication for 3 seconds

Figure 3-16. Optical microscopic image of interdigitated lines. Condition: Figure 3-14 after performing sonication for 6 seconds.

3.1.4 Procedure for reaction chamber

In this section we will describe the process for Polydimethylsiloxane (PDMS) reaction chamber.

Step1. Mixing PDMS and cure agent, the ratio of PDMS to cure agent is 10:1.

Step2. Put in the vacuum pump to degas PDMS and then pour the PDMS to mother mold (shown in Figure 3-17).

Step3. Cure PDMS in hotplate until PDMS is solidified, the temperature is 110°C.

The mold is made of aluminum, the size is 10cm by 10cm square containing 36 cylinders. The diameter of a cylinder is 5mm and the height is 1cm. We can make lots of reaction chamber at the same time by this method. The reaction chamber is open-head in both sides.

Figure 3-17. Photograph of PDMS mother mold.

Below is the process for binding PDMS reaction chamber onto silicon oxide surface of MSM-PD. First put the PDMS reaction chamber in O_2 plasma

(plasma clean PDC-32G) under 2torr pressure with oxygen-assisted. Clean the PDMS chamber under plasma environment for 10mins. Then rinse the PDMS reaction chamber in DI water to active the –OH function group activity[11-12]. Put the PDMS onto the MSM-PD and heat at 90°C on hotplate for 15mins. Figure 3-18 shows the MSM-PD binding with PDMS reaction chamber.

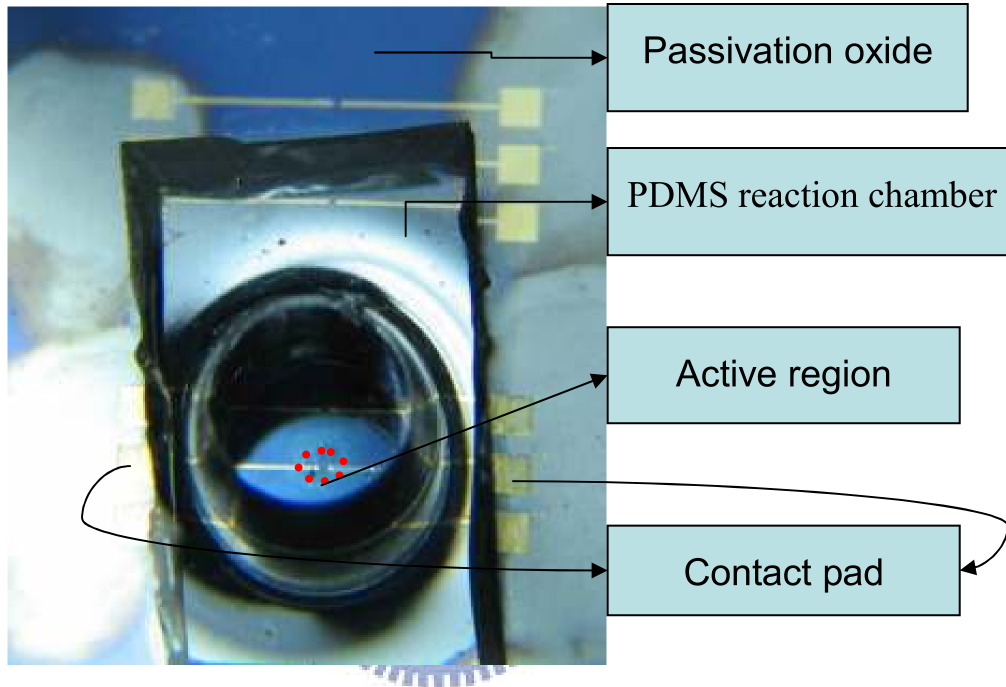

Figure 3-18. Photograph of MSM-PD as on-chip biosensor system.

3.2 Immobilization process (luminol)

All references to H_2O refer to deionized (18 MΩ-cm) water (DI water). Below list the introduction of molecules used in this immobilization process.

(+)-Biotin N-hydroxysuccinimide ester {NHS-Biotin, $C_{14}H_{19}N_3O_5S$; ~98%; Sigma}

This reagent was used for labeling surface functional groups and biologically active molecules such as antibodies, lectins, sugars, nucleic acids or molecules with amino groups. Stored in 4°C.

Phosphate-buffered saline tablets {PBS, 1X; CALBIOCHEM}

PBS, a biological buffer solution, was used to increase the selectivity of the DNA chips by washing away any non-hybridized nucleic acids. This chemical is dissolved in one liter ddH_2O to yield 10 mM phosphate buffer, pH 7.4, 140 mM NaCl, 3 mM KCl.

Streptavidin−HRP from Streptomyces avidinii {essentially salt-free, lyophilized powder, ≥ 5 units/ mg protein; Sigma}

This protein shows high affinity to biotin. The powder needed to dissolve in the PBS prior to use. It must be stored at -20℃.

Step 1. Soak the MSM-PD in piranha solution (H_2SO_4:H_2O_2 = 7:3) at 120°C for 1 hour. Then wash the MSM-PD thoroughly with DI water followed by nitrogen purge.

Step 2. Soak MSM-PD with 10% APTES {(3-aminopropyl)triethoxysilane ; Sigma} in dried toluene for 30mins at room temperature, then washed by toluene and acetone for several times. Dry in an oven for 1 hour. Combine PDMS reaction chamber with MSM-PD

Step 3. Drop 10mM NHS-Biotin (solvent: DMSO) for 6 hours. Washed thoroughly by DI water and then soak in 1% tween-20 solution (solvent: PBS buffer, pH=7.4) for 10 mins. Followed by soaked in BSA solution for 20mins.

Step 4. Soak in streptavidin-HRP solution (solvent: PBS buffer, pH=7.4)

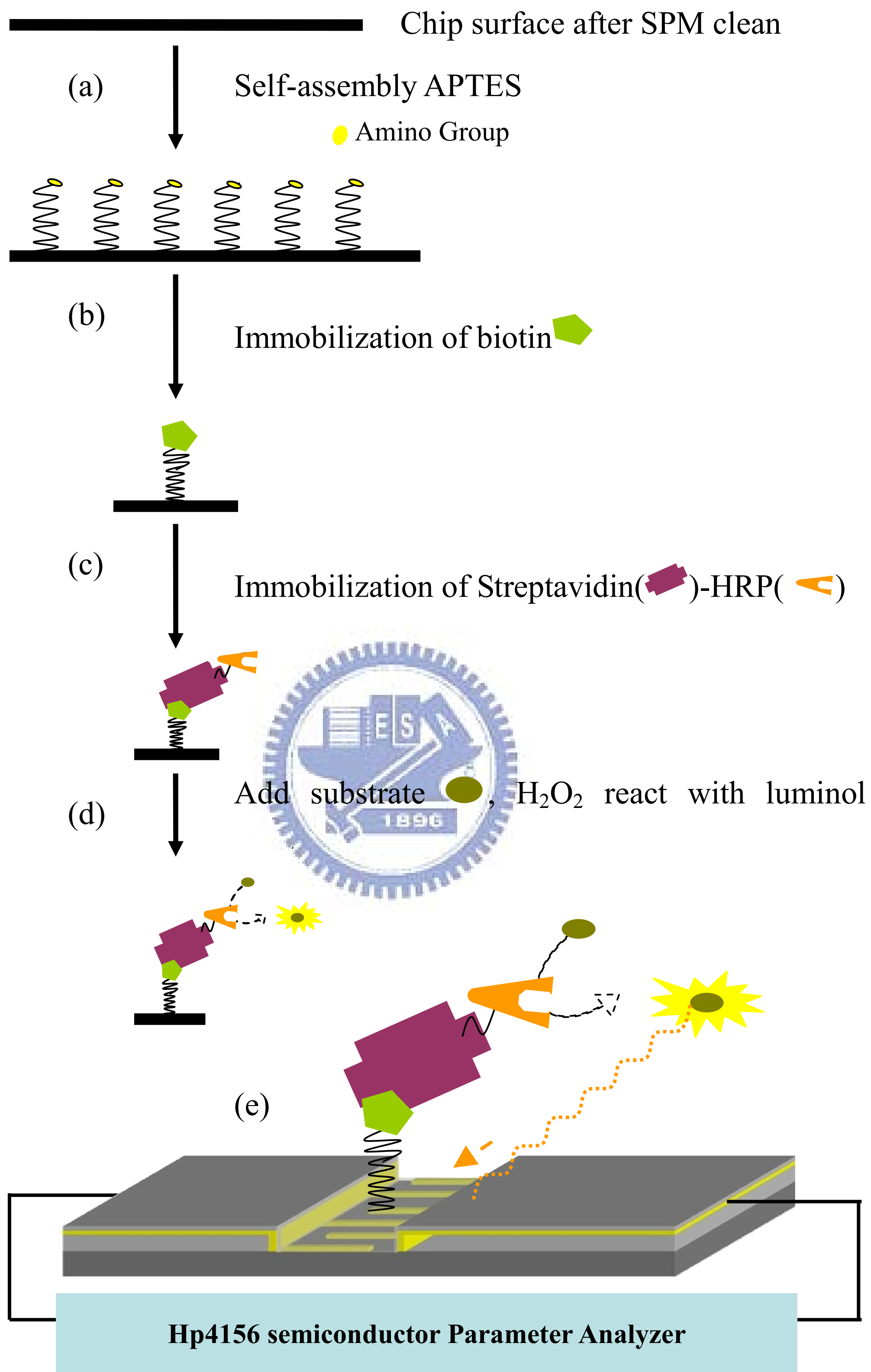

Figure 3-19 Schematic diagram of immobilization process flow

(a) SAM APTES, (b) Immobilization of biotin, (c) Immobilization of streptavidin, (d) Add substrate solution, (e) Schematic diagram of my system.

3.3 Process of gold nanoparticles synthesis

This section will discuss the process for gold nanoparticles synthesis and immobilization of gold nanoparticels onto chip surface.

3.3.1 Gold nano particles synthesis process

Materials: $HAuCl_4$ and Trisodium citrate are purchased from Sigma-Aldrich. All references to H_2O refer to deionized (18 MΩ-cm) water (DI water). The procedure of gold nanoparticles synthesis is below:

Step 1. Heating 1mM 10ml $HAuCl_4$ to 100℃

Step 2. Add 38.8 mM 1ml Trisodium citrate into $HAuCl_4$ solution

Step 3. Waiting for color change from yellow to purplish red

Step 4. Hold the temperature at 100℃ for 15 minutes

Step 5. Cooling down to room temperature then store in 4℃

During the synthesis process we have to put much emphasize on the experimental environment, including container cleaning process, adding reducing agent as soon as possible, and continuously stirring during the synthesis step to prevent aggregation and prevent changing the size uniformity.[13-14]

The mechanism of gold nanoparticles synthesis has two main steps, the first step is nucleation and the second step is growth. In the beginning of reaction the reducing agent will soon transfer Au (III) to many small gold particles. The small gold particles serve as seeds. Once the seeds are accomplished, the amount of the seeds will not change. Then the growth mechanism starts and the oxidation-reduction reaction on the surface of seeds making the gold nano

particles to growth. When Au (III) is completely consumed, the growth mechanism is end up. Trisodium citrate is used as reducing agent, the carboxylic group (COO^-) converts Au^{+3} to Au^{+1} and form acetone dicarboxylate. But how Au^{+1} is transferred to Au is still not confirmed so far. There are two possible arguments about how the Au^{+1} change to Au atom. One is carboxylic group (COO^-) continuously reacts with Au^{+1} to become Au atom. And other argument says that three Au^{+1} ions may form ion-clusters, and perform self-redox reaction to become two gold atoms and one Au^{+3} ion. The reaction is description as below:

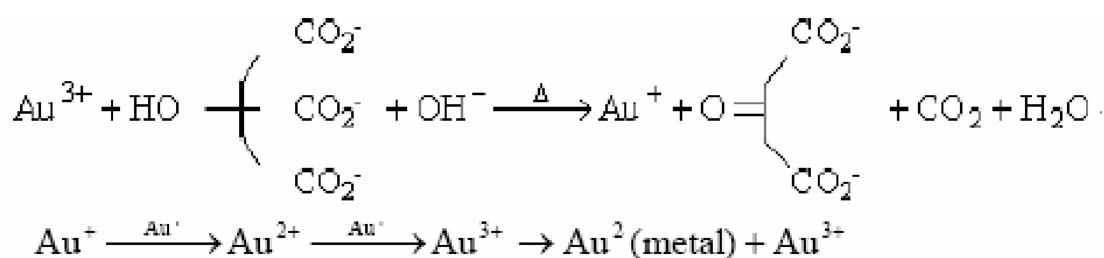

Figure 3-20. The reactions in gold nanoparticles synthesis.

3.3.2 Immobilization of gold nanoparticles

Here is the procedure for immobilization of gold nanoparticles.

Step 1. Rinse the wafer in SPM (H_2SO_4:H_2O_2=3:1) for 10 mins.

Step 2. Rinse the wafer in APTES/EtOH for 40 mins.

Step 3. Rinse the wafer in alcohol and DI water 5 mins respectively.

Step 4. Heating the wafer in hotplate at 120℃ for 30mins.

Step 5. Rinse the chip in the gold nanoparticle solutions for 15 mins. Then wash the chip with DI water and followed by nitrogen purge.

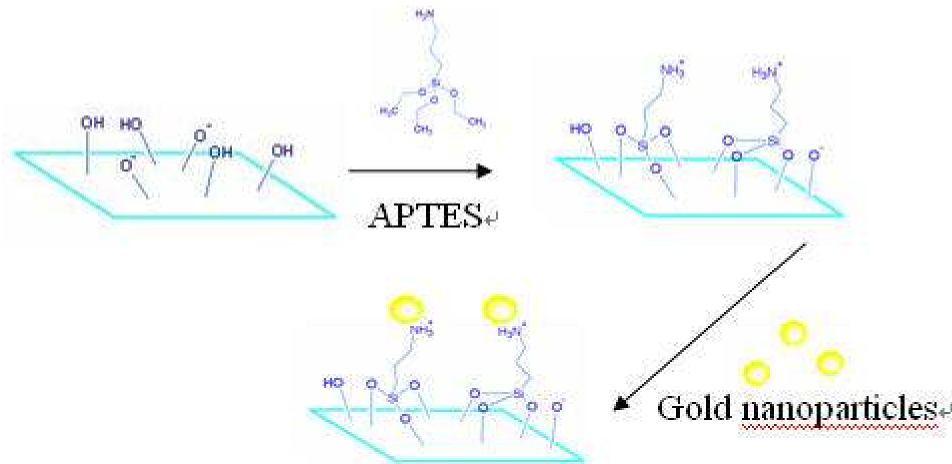

Figure 3-21. The process flow of immobilization of gold nanoparticles.

Prior to immobilization, the pattern sample should be carefully cleaned for 30 min. The temperature of the solution of H_2SO_4 and H_2O_2 (volume ratio is 3:1) must be maintained above 85°C to possess the oxidative power. If the temperature was dropped, hydrogen peroxide was required to replenish. It should be noted that the cleaning solution was very corrosive and dangerous; we must handle it carefully. After pure water rinsing and drying, the pattern of interest was immersed in the APTES solution for 40mins in room temperature. The APTES solution was prepared by the following procedures: (1) mixing pure water with acetone (volume ratio is 5:1), (2) adjusting the above solvent pH to 3.5 by 1M HCl, and (3) preparing the 5% APTES solution by diluting with above solvent. Then, the pattern sample was rinsed with pure water thoroughly. The succeeding step was to bake the chip at 120°C for 30 min.

Chapter 4: Results and discussions

4.1 Device performance

Since our goal is to detect the luminescent light, the photo current (Ip) to dark current (Id) ratio is the main characteristic we will concern with. We focus on this issue in this section. The definition of dark current is the current without illumination, while the photo current is the difference of current with illumination and without illumination.

All the light source I used is halogen lamp from the object lens of optical microscopic and the wavelength is in visible wavelength region. We use a calibration photodiode to measure the power of the halogen lamp. The calibration photodiode has a filter that only wavelength between 300nm~ 800nm can pass through the filter and absorbed by the photodiode. The specification of the photodiode is that 1mA current equals to $100\frac{\mathrm{mW}}{\mathrm{cm}^2}$. The photodiode operates at reverse-biased region. Figure 4-1 shows the halogen lamp power intensity. The lamp has a roll knob to control the power intensity. I make some marks on the roll knob to identify the power level. All the power we use in the following experiments is medium level which equals to $1.46\frac{\mathrm{mW}}{\mathrm{cm}^2}$ if we don't mention specifically. Also since we don't have a coherent laser, we can't calculate the quantum efficiency for specific wavelength.

The conventional MSM-PD is without anti-reflection layer covering. For immobilization surface requirements we deposit silicon oxide onto the active area. The silicon oxide thickness is also designed for optimal anti-reflection design here. The thickness of the anti-reflection coating was calculated using

$T_{SiO2}=[\lambda_o/4n(\lambda)] \bullet m$

T_{SiO2} is oxide thickness, λ_o is incident wavelength, $n(\lambda)$ is oxide index of refraction of wavelength, m is any odd integer[1]. After calculating the T_{SiO2} is about 76nm for 450nm incident light. Here I will compare the photo response before and after depositing oxide anti-reflection layer.

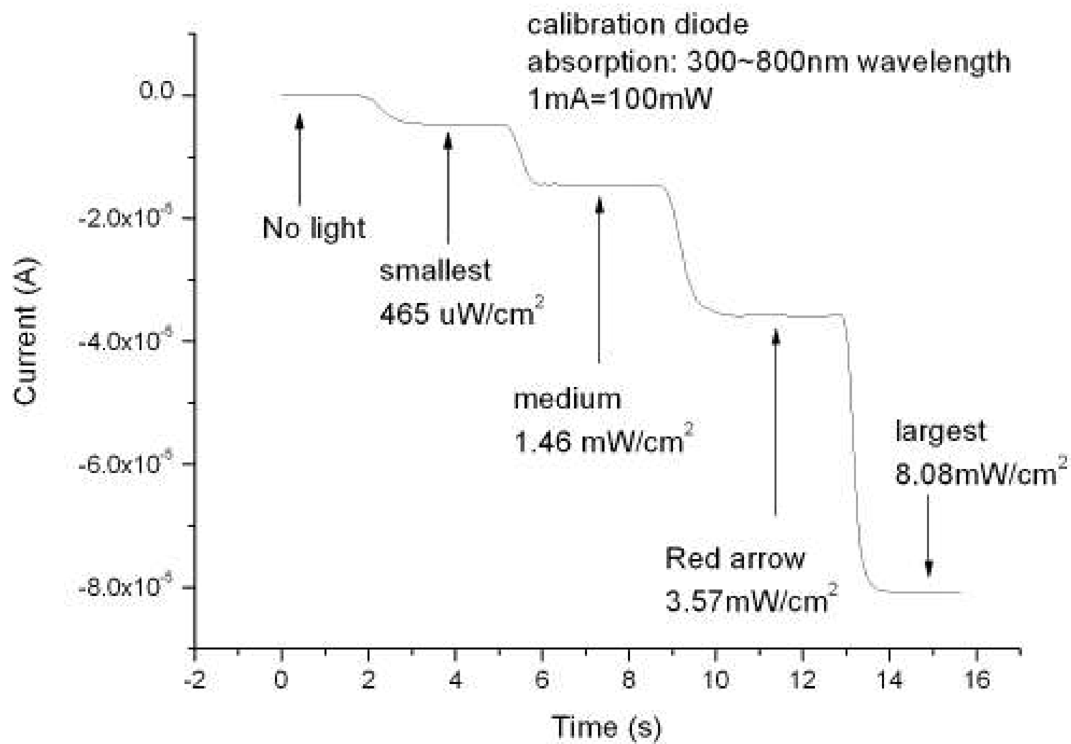

Figure 4-1. Power intensity of halogen lamp measured by calibration photodiode.

4.1.1 Photo response without anti-reflection layer

Figure 4-2 shows the photo current to dark current ratio operation at 7V is 216. The photo current is 0.4uA at 7V and the dark current is 82.27uA. In the small voltage region (~1V) the electric field generated by applied voltage may not strong enough to separate the photo-induced electrons. As the applied voltage gets larger and larger the corresponding electric field is stronger, hence it

can collect more electrons resulting in large photo current.

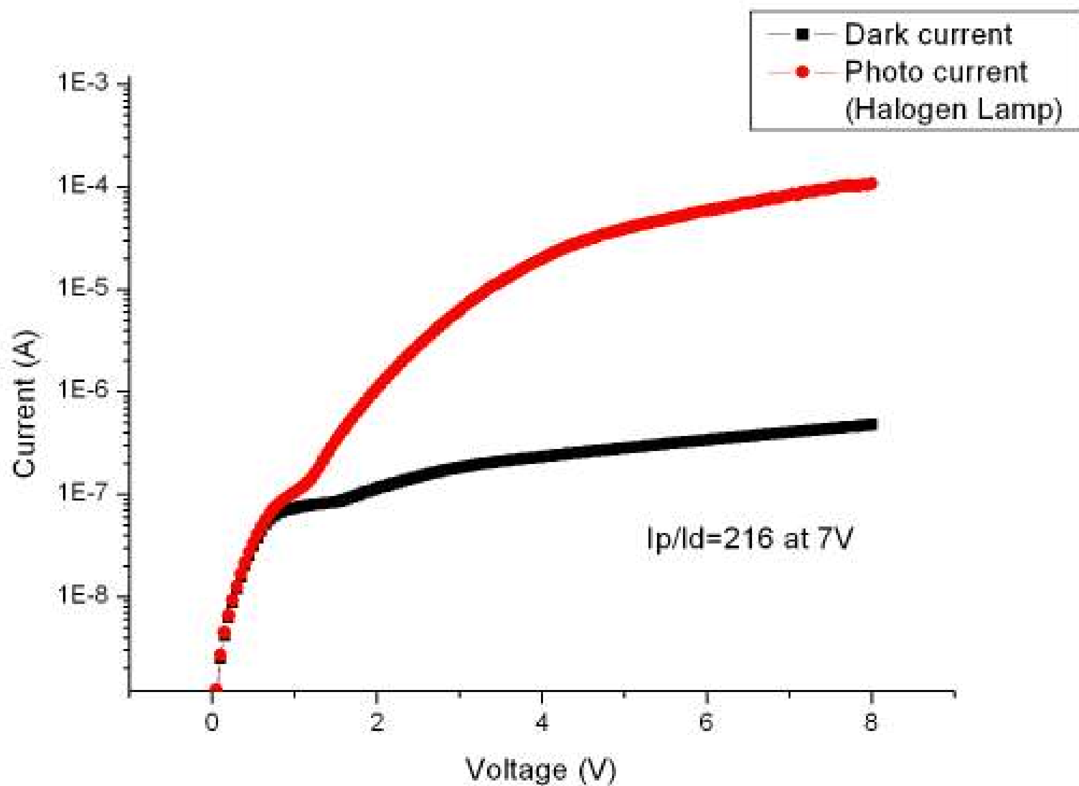

Figure 4-2. I-V characteristic before deposition of oxide anti-reflection layer.

4.1.2 Device stability

Afterward we measure this device for 10 times to check the device stability. As shown in Figure 4-3 , the line is average current signals and the error bar is triple standard deviation. Because each device may have distinct photo response duo to different profile of interdigitated lines and different quality in schottky contacts. We will test each device to pick out the optimal operation voltage which contains the largest photo current to dark current ratio and the smallest deviation in dark current. By statistical analysis we know that about 99.7 % lie within triple standard deviation. Photo current signals must obtain larger than the average dark current plus triple standard deviation for validity. This is very important point in the following applications.

In this device we can find out the device is considerably stable, the value of triple standard deviation is 14.2nA operation at 7V and the average dark current is 417nA. It's around 3.4% difference between the triple standard deviation and the average value.

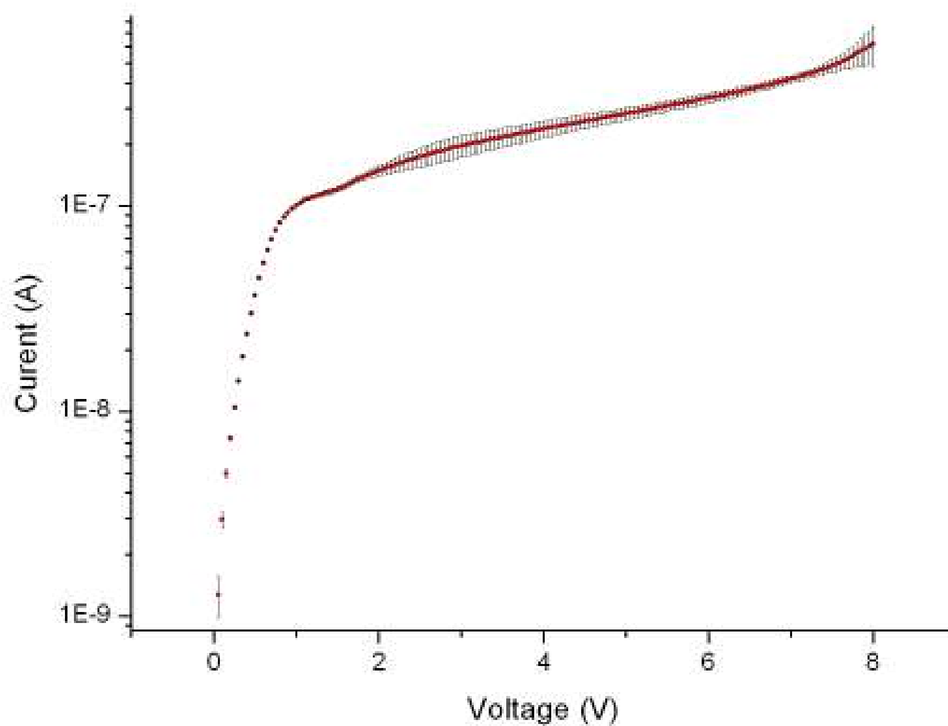

Figure 4-3. I-V characteristic indicates the device is stable. The measurement of dark-current for 10 readings, the curve is the average value and the error bar is triple standard deviation.

4.1.3 Symmetric characteristic of MSM-PD

By the name of Metal-Semiconductor-Metal photodetector, we can identify clearly that when electrons flow through MSM-PD will encounter two schottky barriers. No matter the device is operated at the positive or negative voltages, the electrons generated in semiconductor region are collected by adjacent metals. The electrons all pass through the same path but in different directions. I-V

curve in Figure 4-4 shows the symmetric characteristic of MSM-PD. The operation voltage either in positive or negative doesn't affect the photo-current to dark-current ratio, so I will measure only one side of operation voltage in the following experiments.

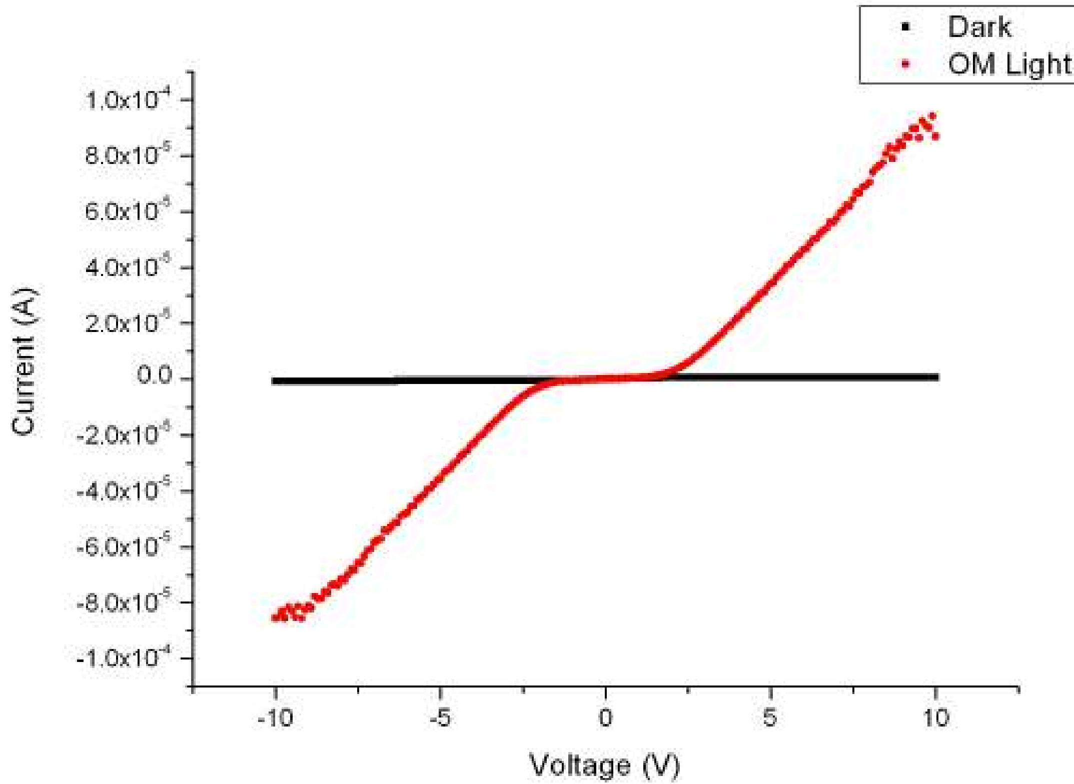

Figure 4-4. I-V characteristic: Symmetric characteristic in positive and negative voltages.

4.1.4 Photo response with anti-reflection layer

After depositing silicon oxide layer which serves as anti-reflection layer, the photo current to dark current ratio can further improvement to 3 orders of magnitude. We can see the reflection data by N&K analysis in Figure 4-6. In the visible light wavelength 300nm~800nm, the reflectance are significantly drop, thus giving more incident light striking on the absorption layer.

The luminescent light has emission peak at 450nm while gold nanoparticles

have absorption peak around 520nm (the following applications will focus on these wavelength). By N&K analysis we can see the reflection of silicon is 42% at 450nm while 38% at 520nm, and the reflection of silicon oxide is 20.1% at 450nm while 12.5% at 520nm.. Simulation result tells us the best reflection of mono-layer anti-reflection by silicon oxide at 450nm is around 17%, a little better than ours. It may because that the oxide layer is deposited by PECVD, and the thickness may not exactly what I expected because of the limitation of this equipment. The sample in Figure 4-5 contains 90nm silicon oxide thickness. We all know metals have large reflectance. The oxide layer depositing onto gold also enhance the transmit light in gold electrode areas.[2] This also decrease the shadow effect[3] and further improving conversion efficiency of anti-reflection layer. There may have another effect can enhance the reflection in our device structure. This is "textured effect", which means pattern the anti-reflection layer. In the MSM-PD, the silicon oxide is deposited onto interdigitated lines. So the oxide surface isn't planar, the surface may have periodic pattern like grating (300nm grating which is sub-wavelength structure), thus result in textured surface. This effect leads to lower reflection than planar structure.[4] The textured surface can decrease much reflectance, and is well used in solar cell industry. The famous one is pyramid-shape anti-reflection structure can further depress the reflection below 10% [5]. Another advantage of textured surface in depressing reflectance is that the textured surface unlike planar structure anti-reflection only optimal for a specific wavelength, it can lower the reflection over a wide range of wavelength [6]. The goodness of "textured effect" and "shadow effect" is not indicated in N&K data, because the active area is smaller than the light spot of N&K. Figure 4-6 only indicates the differences of reflection between oxide/silicon and bare silicon.

In addition to the benefit of anti-reflection, there might be another benefit enhances the photo current to dark current ratio. From Figure 4-6 we can see the dark current is much lower than before depositing oxide layer. As we know when insulator is sandwiched between two metals, it will form capacitors also known as metal-insulator-metal capacitors (MIM). After deposition of silicon oxide, our devices have lots of metal-oxide-metal capacitors. These capacitors may trap and storage electrons which lower the dark-current as well as the photo current.[7] This may be the reason why dark current and photo current both drop after deposition of oxide layer.

At 5V applied voltage the dark current increasing rapidly may because of capacitors breakdown, the distance of two adjacent electrodes is 300nm. From V=E*D, where V is the potential difference between two electrodes, E is the electric field, D is the distance between two adjacent electrodes. After calculation the electric field is $1.67*10^5$ (V/cm). We also mark that photo current maintains nearly constant value in the saturation region without rapidly increasing. Breakdown of capacitors causes increasing current may because of releasing the trap electrons. The formation of capacitors also enhance the performance of our MSM-PD.

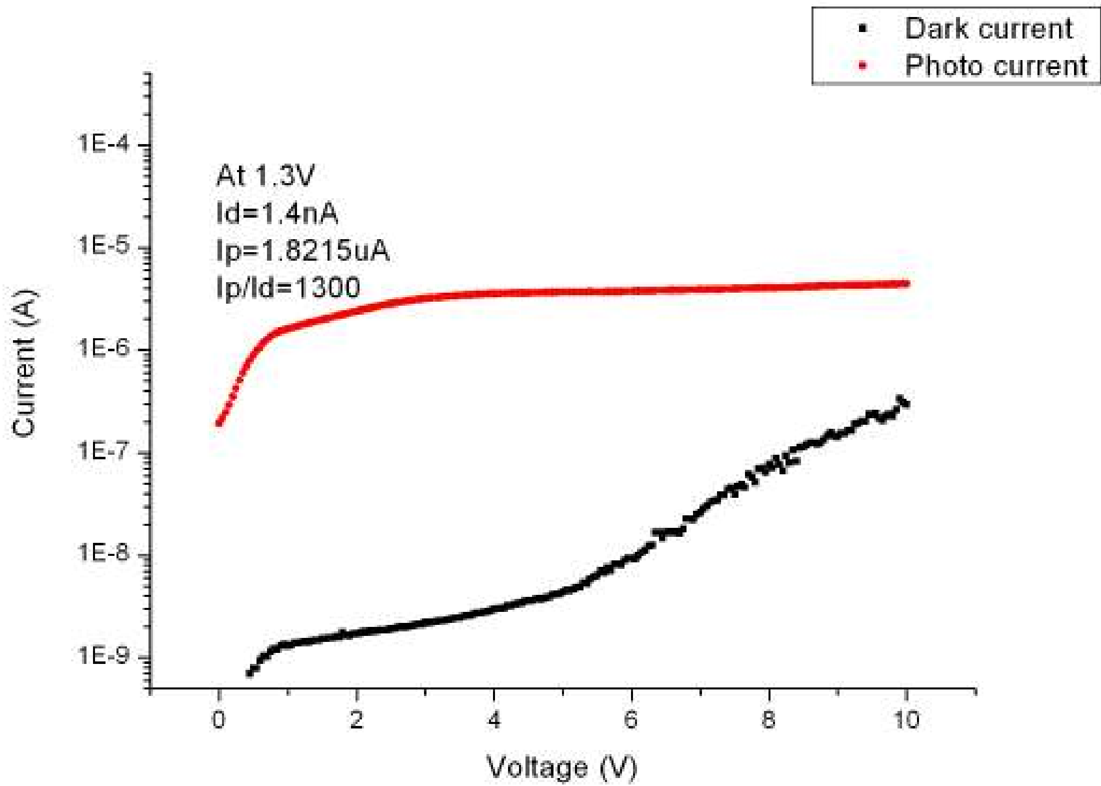

Figure 4-6. I-V characteristic after deposition silicon oxide layer.

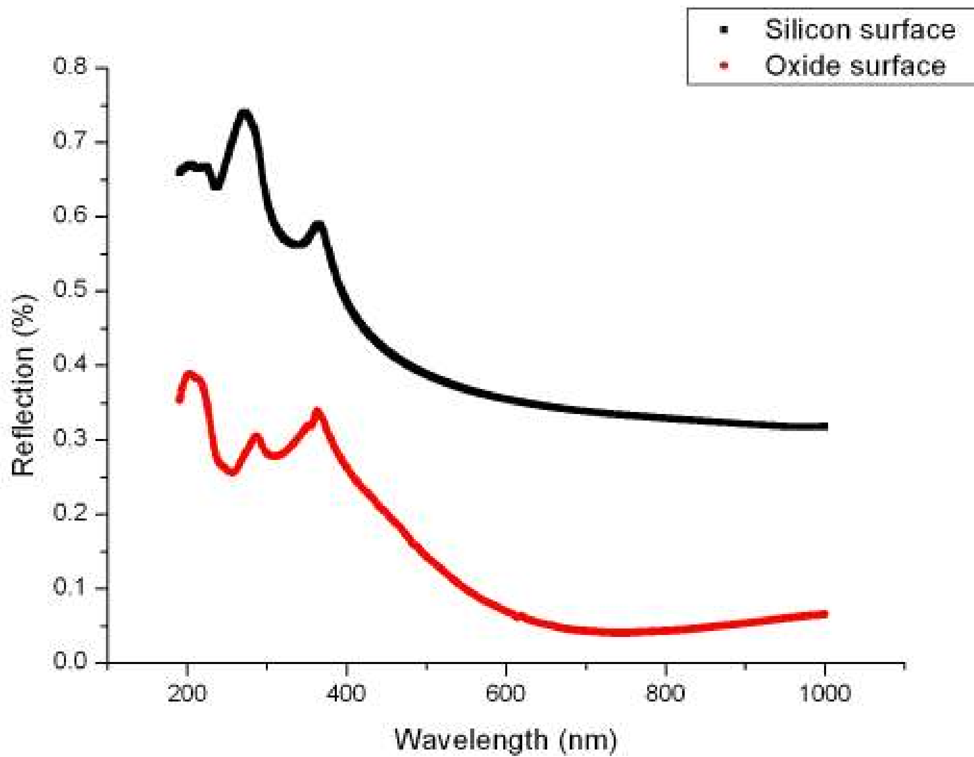

Figure 4-5. The analysis of anti-reflection result by N&K.

4.1.5 Sampling mode measurement

Figure 4-7 shows the sampling mode of MSM-PD. The power intensity of halogen lamp is modulated at the smallest power. The dark-current is 1.43uA and the photo current is 23.7uA. We can't measure the transient time because we don't have pulse generator to turn on and off the light source. We just can manually control the roll knob of halogen lamp to turn it on and off, it takes much more time than pulse generator. The slope relates to the speed that I rolling on/off the roll knob. During the time interval of 0~0.8s the lamp is off and the dark current is fairly stable. Then we turn on the lamp at 0.8s, the photo current reaches the maximum at 1.8s. We turn off the lamp at 2.3s and at 3.8s the current drop to the dark-current as before. According to researches in transient time response of MSM-PD, the Fall-time is in the range of tens of pico-second in amorphous silicon based MSM-PD.[8] Theoretically, the narrower distance between two metals can have better performance in transient response. Due to lacking pulse generator we can't do this measurement. But it doesn't matters because that my experiments focus on the photo current to dark current ratio, not on fast transient time in the following applications. This test is just to verify that MSM-PD can function well on continuous measurement and the dark-current and photo current remains constant.

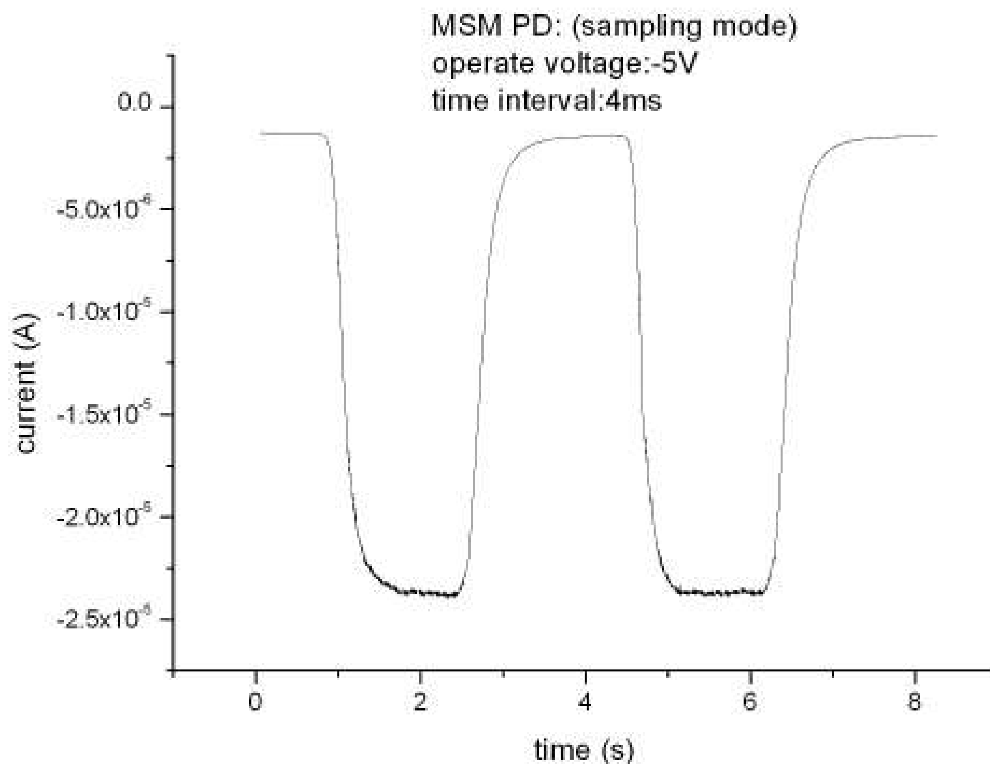

Figure 4-7. Sampling mode of MSM-PD. The device operation at -5V and the time interval is 4ms.

4.2 Luminescence application

In this section, we will demonstrate the MSM-PD for detection luminescent light. We demonstrate MSM-PD to detect the light emission from the streptavidin-HRP catalyzed luminescent reaction. By detecting streptavidin concentrations, we can also detect molecules that can bind onto it.

The detailed experimental process flow is expressed earlier in chapter 3.2. We will show the I-V characteristic of each step here. The MSM-PD is operated at sampling mode for real time measurement. Halogen lamp serves as the light source and the power is applied in medium level. (The halogen lamp is for making sure our device still alive)

4.2.1 Real-time sensing for Luminescence

This section we will apply MSM-PD as biosensor for luminescence detection. First we have to make sure the silicon oxide layer can completely avoid electrolysis in liquid solutions. In active area the metal lines are very close to each other, and after apply electric potential on the metal pads it will make strong electric field between adjacent metal lines. Electrolysis will provide another current path thus increasing the dark current of the MSM-PD. The photo current to dark current ratio will be significant drop resulting in that photo current can't be recognized. The device is operated at 0.4V, and the light source is halogen lamp. The immobilization processes are all performed in reaction chamber (except for APTES) thus will not change the contact resistance between probe and pad. Why we measure photo response in each step is to ensure the device still works after each immobilization step. After SPM clean, the dark current is 2nA and the photo current is 1.152uA. After immobilization of APTES the dark current slightly increases to 3.7nA, and the photo current is 193nA. The photo current drop so much may because of oxide chamber blocking some incident light, and the measurement is under liquid solutions (PBS solvent). The solutions will also absorb some incident light. The photo current is not what we concerned with here, just to ensure the device is still alive. The dark current increases a little may because some leakage current results from oxide surface. The silicon oxide is deposited by PECVD, there may have some metal contamination and lots defects. Some ions in the liquid solutions near on oxide surface may exchange electrons and the electrons diffusion through defects in oxide layer then collected by metal electrodes. The leakage current causes dark current to increase a little. All the following measurement is under liquid

solutions (PBS). The dark current is still 4nA after immobilization of biotin and streptavidin. After adding substrate solutions (Chemiluminescent Peroxidase Substrate for Western Blotting; Sigma), it will emit a very weak light. The mass of streptavidin is 5ug, and the total solution volume is 200mL. Why the current doesn't go back to 4nA is because that luminescent light can continuously emit for about 30 mins, but I only measure 4mins.

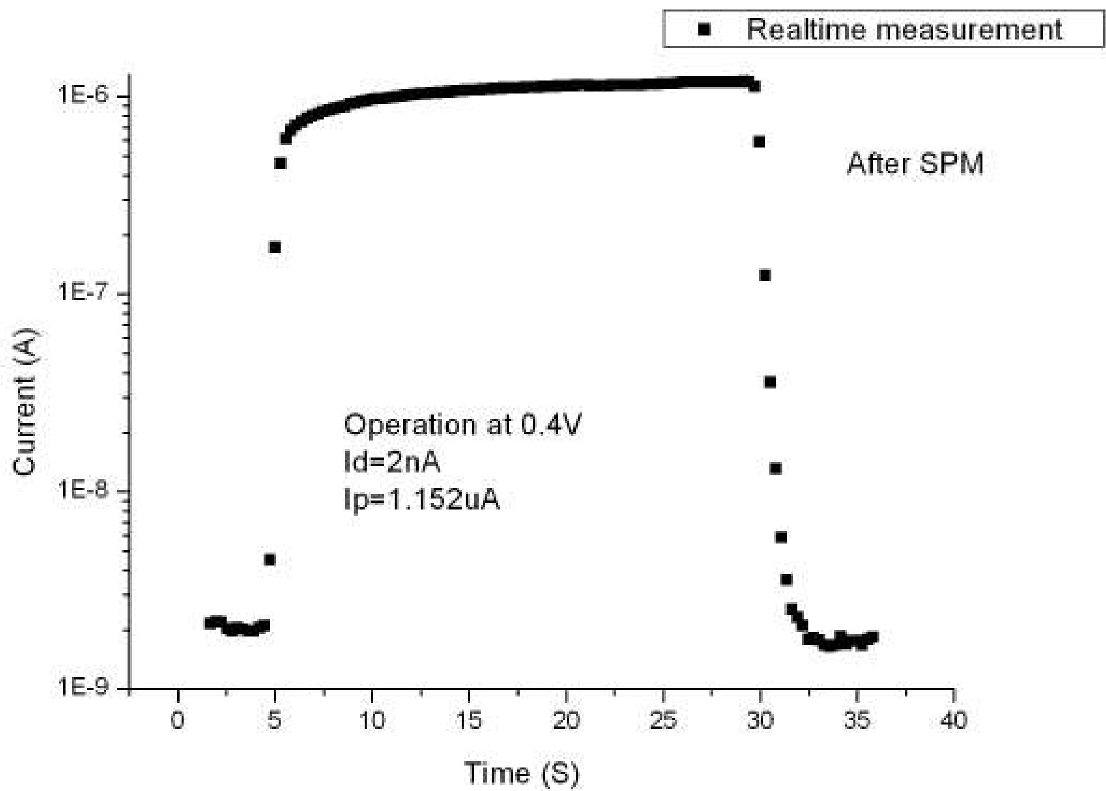

Figure 4-8. Sampling mode of MSM-PD after SPM clean.

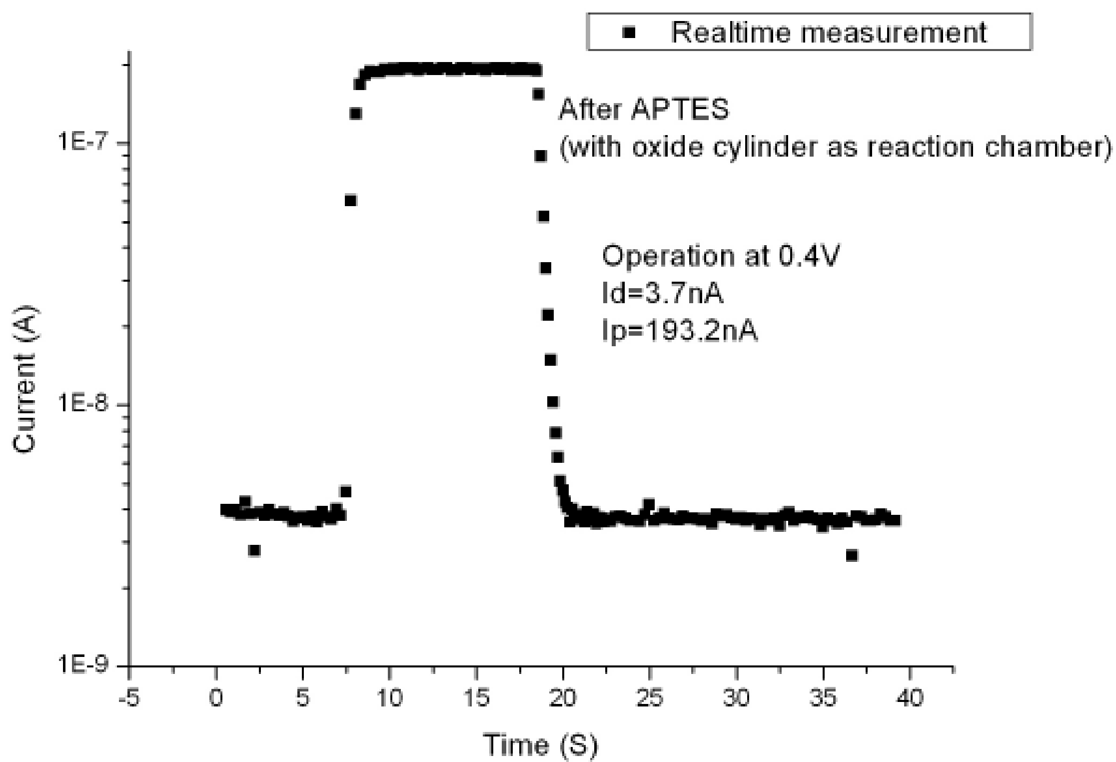

Figure 4-9. Sampling mode of MSM-PD after immobilization of APTES.

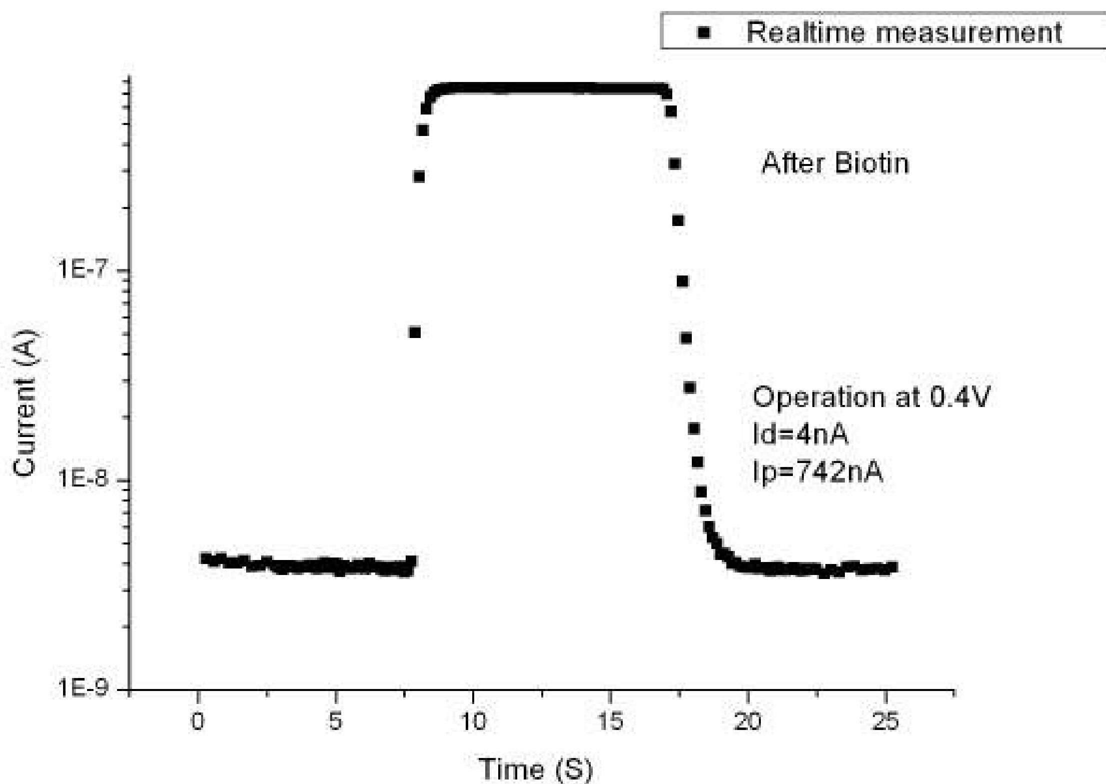

Figure 4-10. Sampling mode of MSM-PD after immobilization of biotin.

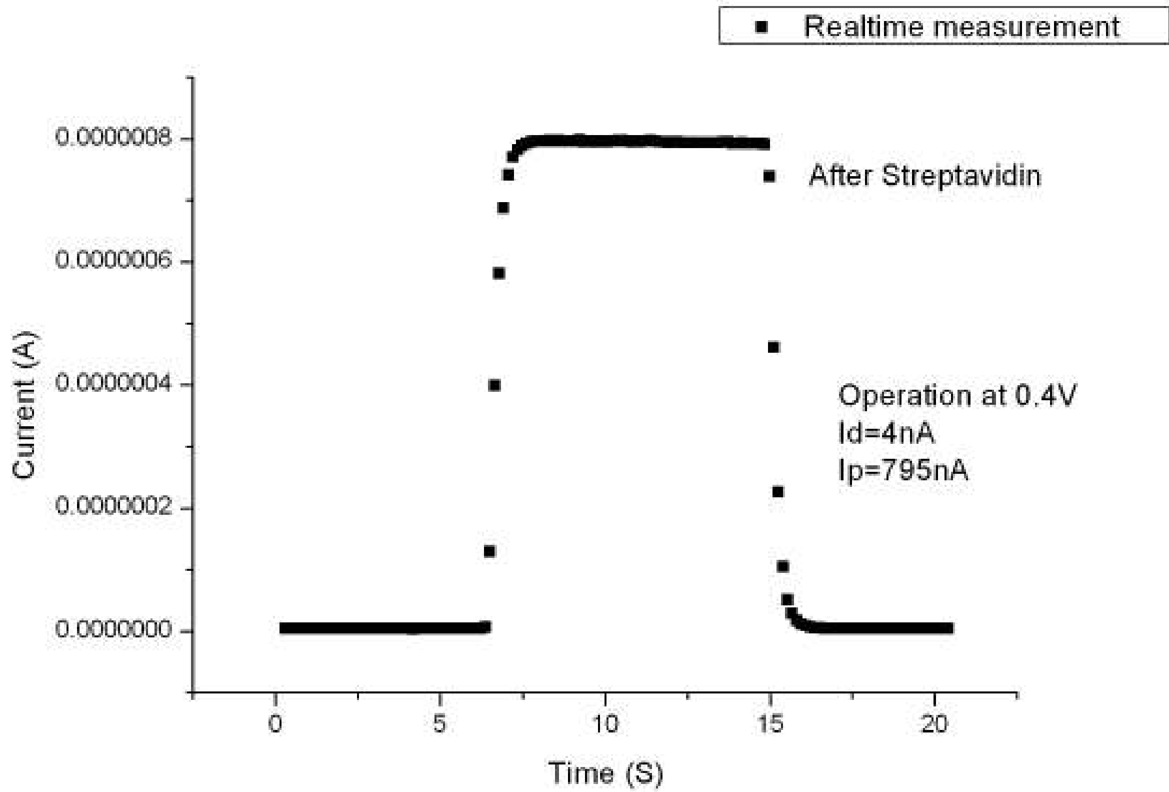

Figure 4-11. Sampling mode of MSM-PD after immobilization of streptavidin.

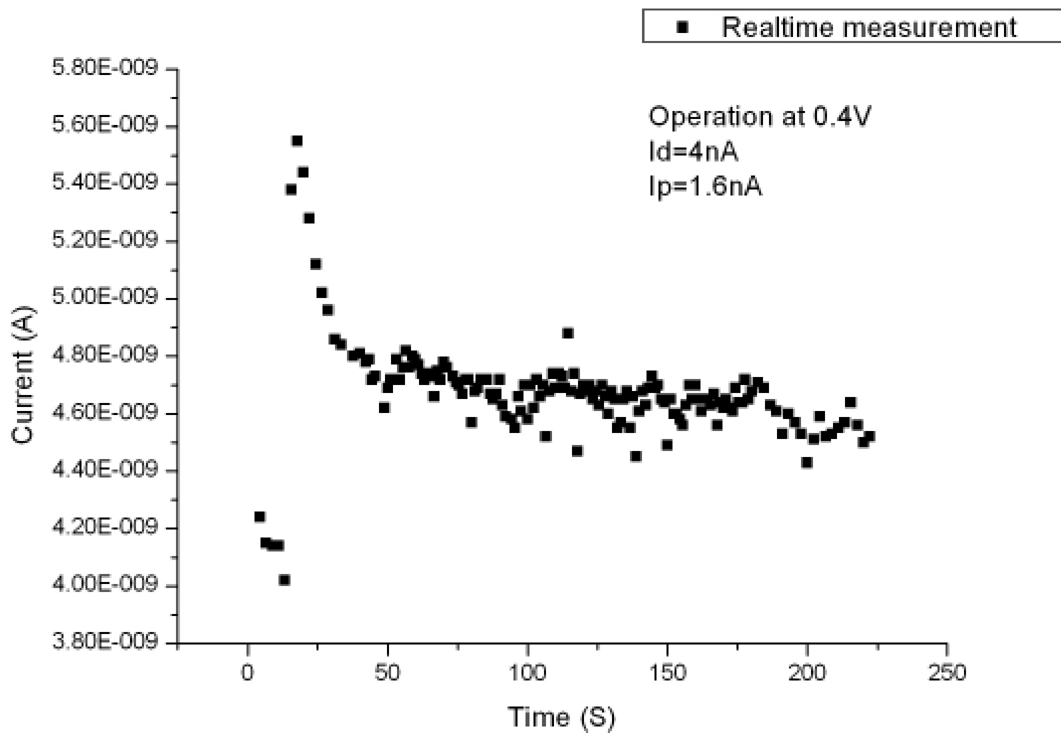

Figure 4-12. Real-time measurement after add substrate. (Immobilization of

streptavidin-HRP catalyzed luminescent system)

4.2.2 Calibration line and minimum detection limit

Above experiments are immobilized on silicon oxide surface. In this section we will show the device for detecting different streptavidin concentrations and further complete the calibration curve. Because different devices may not have the same photo response, thus the calibration curve must be made by the same device. For safety consideration, we use non-immobilization instead of immobilization, because the device may fail or photo response may change during repeated immobilization process. In this experiment we use PDMS as the reaction chamber and total volume is 100uL. I change streptavidin concentration from low to high, and use PBS solutions to clean the chamber thoroughly avoid streptavidin-HRP residues. The amount of substrate is overdose than streptavidin to provide continuously luminescent reaction. The scale of x-axis is time and before zero second the signal is dark current while after zero second the signal is luminescent light current. The device operates at 0.4V and scanning time interval is 0.5ms. We select the largest current as the photo current and then divide by dark current as the photo response. The photo current to dark current ratio is 1.3, 3.4, 21 in Figure 4-13, 14, 15, respectively. The lager concentration of streptavidin will provide more enzyme (HRP) to catalyze the reaction and have more emission light thus the photo current to dark current ratio will be larger. MSM-PD has a special characteristic that is power linearity [9-10]. In certain power region, the photo current to dark current ratio is proportional to incident light power. In order to make the calibration line, we combine the immobilization data listed in chapter 4.2.2. According to out previous investigation on immobilization efficiency, we assume the immobilization

efficiency is about 1%. The photo current to dark current ratio is 0.4 when streptavidin mass is 50ng. The x-axis is the streptavidin mass while the y-axis is the photo current to dark current response. Figure 4-16 shows the photo current to dark current ratio is nearly proportional to streptavidin mass. The luminescent reaction is first-order [11], thus the emission light is proportional to the amount of enzyme binding on streptavidin. It also points out the MSM-PD have good power linearity in this power range. Also by linear fitting we acquire the relation between photo current to dark current that y=0.0218x-0.8378, y is photo current to dark current ratio, x is streptavidin mass. The regression coefficient is 0.9999 proves the calibration line is very precision. By the calibration line we can exactly know the streptavidin mass inside reaction chamber. As a biosensor, we can detect the disease molecules biding on streptavidin to acquire the concentration of the disease molecules. This process time is extremely short, the data can be immediately acquired. Besides, the device can be used for a few times after clean thoroughly.

The dark current is the noise signal in this system. Figure 4-17 shows the dark current signals. With further analysis the average dark current is 0.449uA, and the triple standard deviation is 0.03nA. Statistical theory tells that about 99.7% lies within the triple standard deviation, and I take the average dark current plus triple standard deviation as the minimum detection limit. The photo current signal will be valid when excess this value. Thus I get the minimum photo current to dark current ratio is 0.22. From y=0.0218x-0.8378 (in Figure 4-16), we know the y is 0.22, by simple calculation can get the minimum streptavidin mass is 4.9ng.

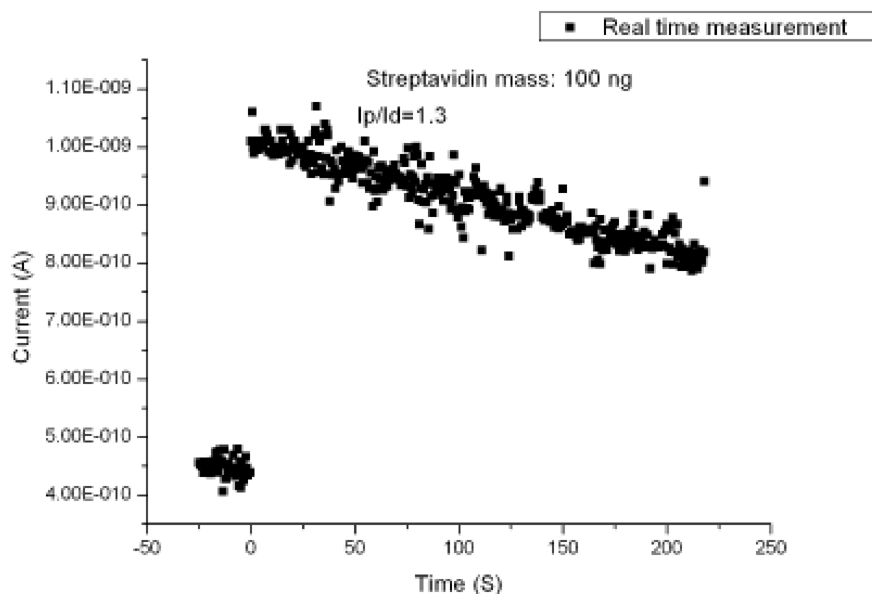

Figure 4-13. Real-time measurement for non-immobilization luminescence. The mass of streptavidin is 100ng and dissolved in 10uL PBS solutions, and substrate solution is 90uL.

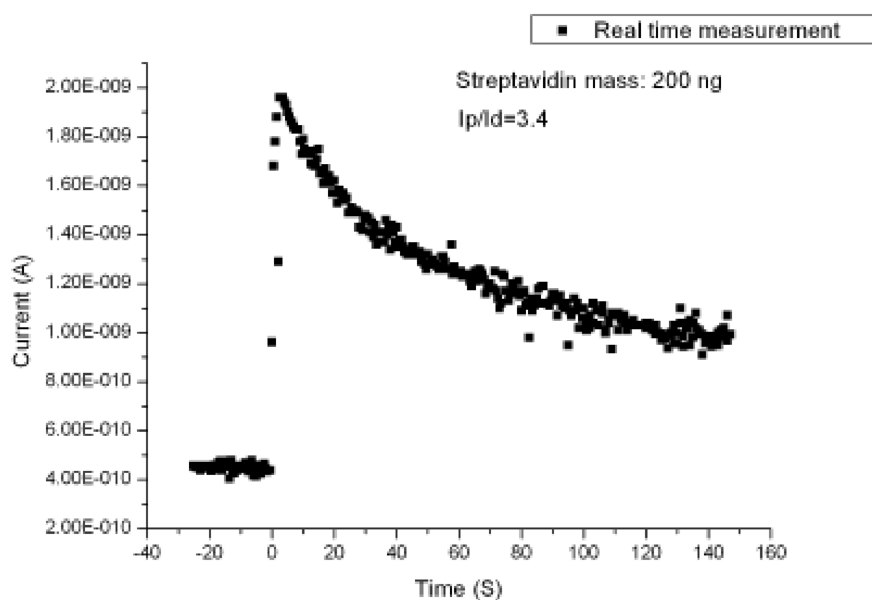

Figure 4-14. Real-time measurement for non-immobilization luminescence. The mass of streptavidin is 200ng and dissolved in 20uL PBS solutions, and substrate solution is 80uL.

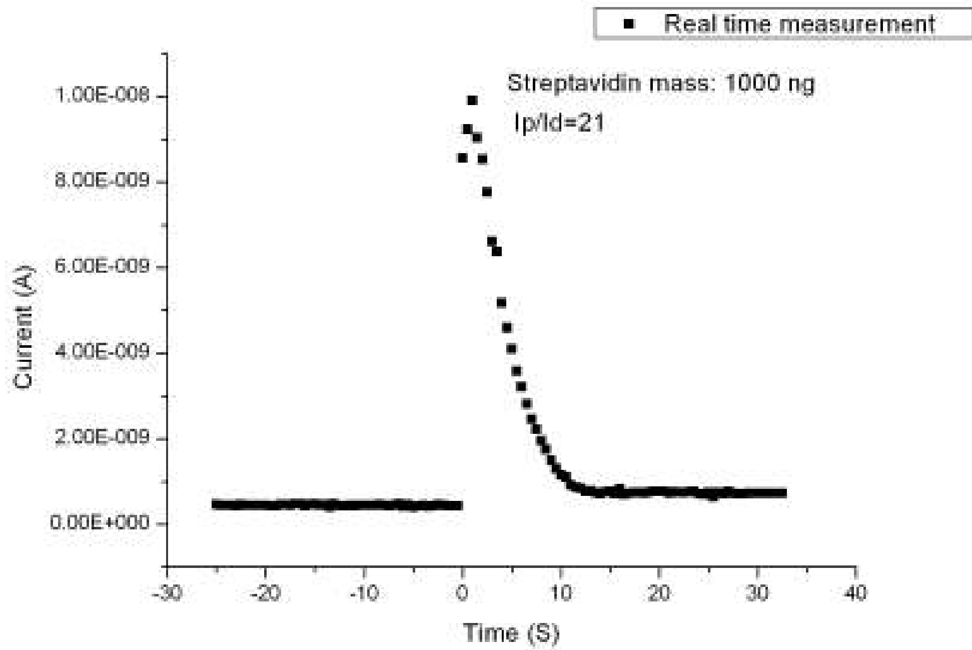

Figure 4-15. Real-time measurement for non-immobilization luminescence. The mass of streptavidin is 1000ng and dissolved in 10uL PBS solutions, and substrate solution is 90uL.

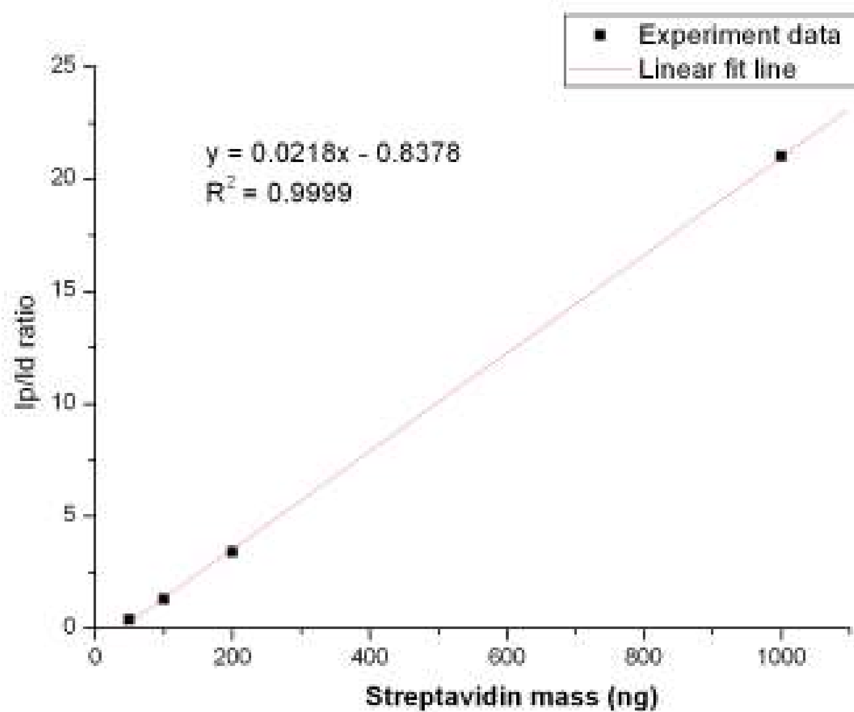

Figure 4-16. Calibration line of MSM-PD on-chip biosensor.

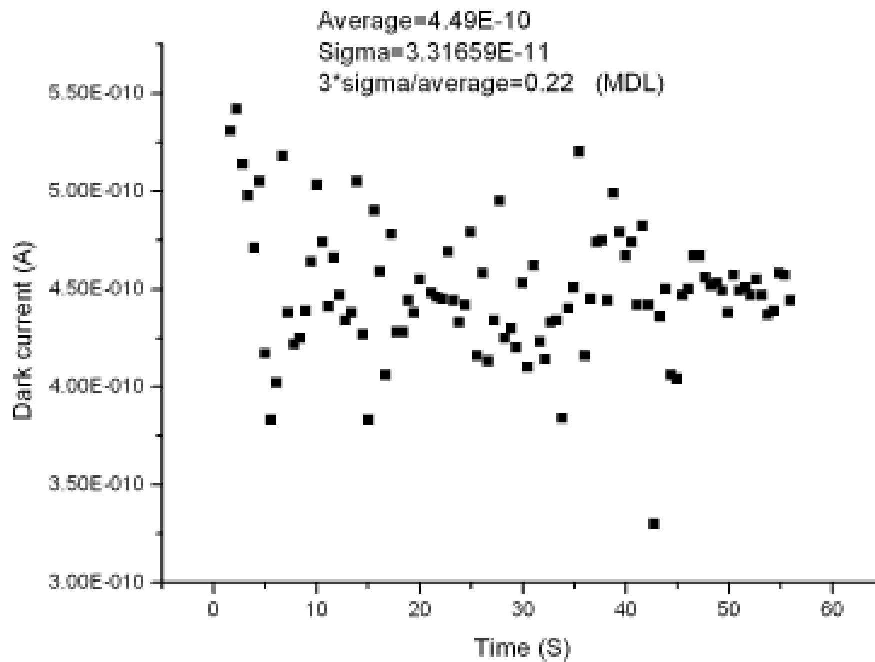

Figure 4-17. Dark current (i.e. noise single) under PBS solution of the MSM-PD on-chip biosensor.

4.2.3 Average molecules per unit area

Nowadays single molecule detection is a very hot topic. We want to know how many molecules are immobilized on the oxide surface. Combine with immobilization data and calibration line, we believe the assumption of immobilization efficiency is about 1% is properly, so there are 50ng streptavidin binding on the oxide surface. The key point in luminescence is the enzyme biding on streptavidin. The mass of streptavidin molecule is 60kD while horseradish peroxidase (HRP) is 44kD. The binding ratio between streptavidin and HPR is unknown, and we do the worst assumption that streptavidin to HRP binding ratio is 1:1. Since I have the single molecule mass (104KD) and total mass (4.9ng) and 1KD= 1.66053886×10^{-27}Kg. Thus there are 2.8373×10^{10} molecules inside the PDMS reaction chamber and the binding areas of silicon

oxide is $0.1963495 cm^2$. After simple calculation density is 1.445×10^{11} (molecules/cm^2). This is far beyond single molecule detection. But the minimum detection limit of my MSM-PD can still apply for much disease detection. [12]

4.3 Gold nanoparticle detection

First we use SEM to look over the results of immobilization of gold nanoparticles. Figure 4-18(a) shows that the gold nanoparticles are immobilized perfectly on the silicon oxide surface. The uniformity and the size distribution of gold nanoparticles are both great. The average size of gold nanoparticles is 13nm in Figure 4-18(b). This is analyzed by the software named Image-pro plus (IPP), and the analysis region is the full SEM image.

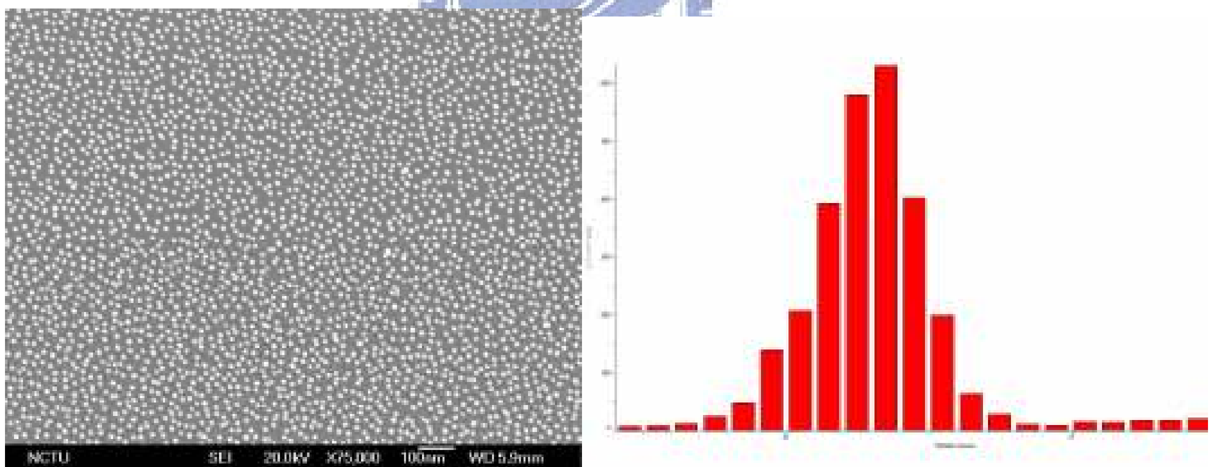

Figure 4-18. (a) SEM image of immobilization gold nanoparticles onto the oxide surface, (b) static analysis of gold nanoparticles size distribution by IPP software.

Figure 4-19 shows the device operates at 2V and the dark current is 25nA, the photo current is 4.5834uA, after immobilization of APTES. The light source

is halogen lamp and the power is in medium level. Figure 4-20 shows the dark current is 15.9nA and the photo current is 2.4612uA after immobilization of gold nanoparticles. The dark current is not similar to each other because the contact resistance may alter due to different probing position resulting in different contact resistance. We can see the photo current to dark current ratio drop from 183 to 154 after immobilization of gold nanoparticles. The decreasing rate is 15.9%.

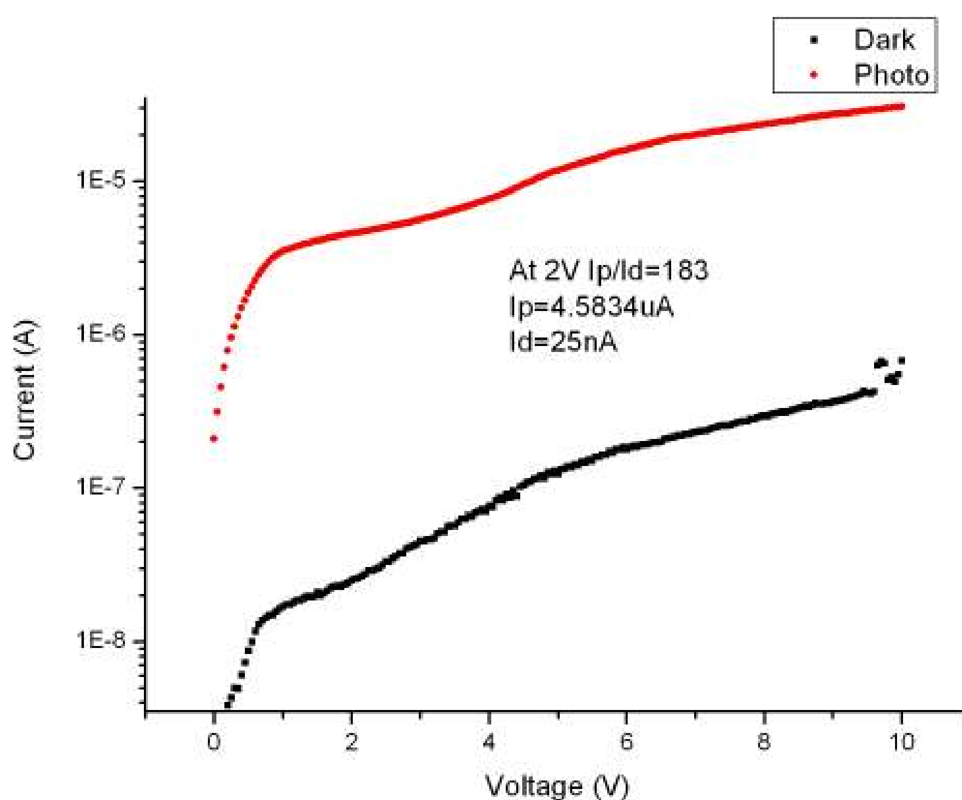

Figure 4-19. I-V characteristic of the device after immobilization of APTES (Sweep mode).

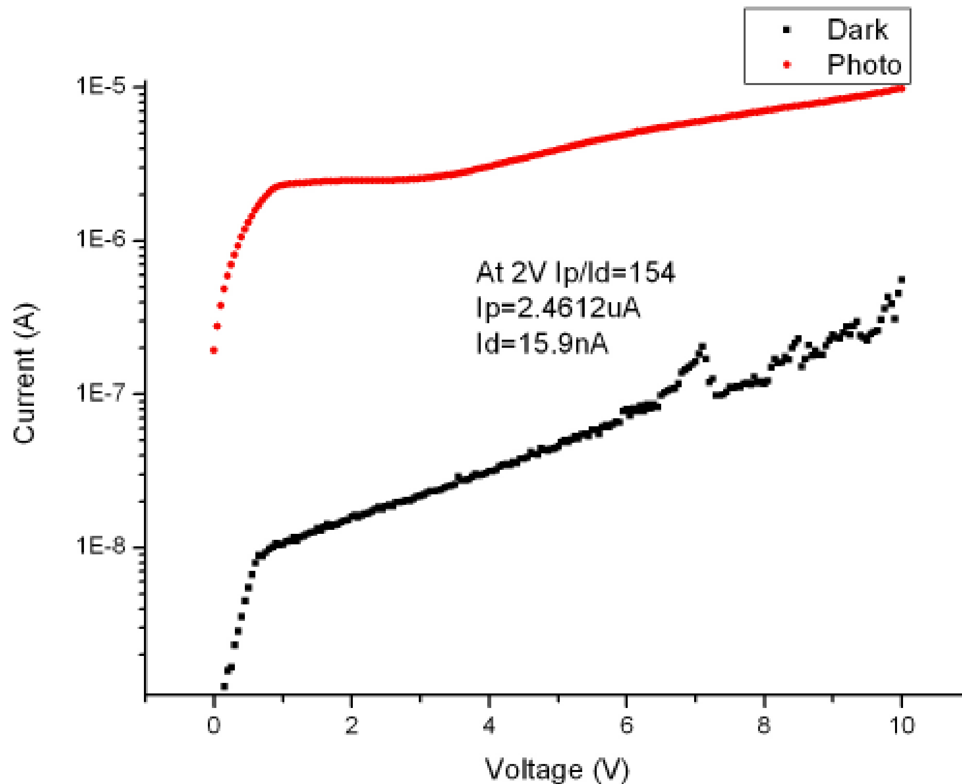

Figure 4-20. I-V characteristic of the device after immobilization of gold nanoparticles (Sweep mode).

As we anticipation the gold nanoparticles have absorption peak around 520nm wavelength. From optical physics we know when light incident onto a surface, there will be transmittance, reflectance, and absorption by medium in the interface. The sum of transmittance, reflectance, and absorption will be the same as incident light. We use UV-Visible to get the absorption of gold nanoparticles. And we use N&K to get the reflectance data in each step. We dissolve the gold nanoparticles in DI water and check the UV-Visible. There is an absorption peak at 518.5nm (Figure 4-21). Then we compare the reflection of the surface after each step (Figure 4-22). After immobilization of APTES, the reflection is almost the same as the reflection of silicon oxide surface. The reflection of gold nanoparticles is a little difference in the range of 240nm to

330nm. The absorption layer of our photodetector is single crystalline silicon, and this absorption layer is almost transparent to UV light. So it is not the key point that affects the photo current to dark current ratio. As mention earlier that I=T+R+A, I: incident light; T: transmittance; R: reflectance; A: absorption in the medium. Our device measures the transmission light. UV-Visible measures the absorption light in gold nanoparticles. N&K measures the reflection light. The incident light is the halogen lamp and the power level is maintained constant. The lower photo current is because of less transmission light absorbed by gold nanoparticles. Since the reflection part of APTES and gold nanoparticles is in the same in visible wavelength region. The data of UV-Visible points out the main reason is because of gold nanoparticles absorbing light. Gold nanoparticles have an absorption peak in 518.5nm leading to less transmission light. The suface plasma resonance will also happen in the interface of gold nanoparticles and oxide, and the absorption peak will shift in different wavelength. [13-14] Thus in the reaction chamber the gold nanoparticles have two kinds of SPR: one is gold nanoparticles and DI water interface, the other is gold nanoparticles and oxide interface.

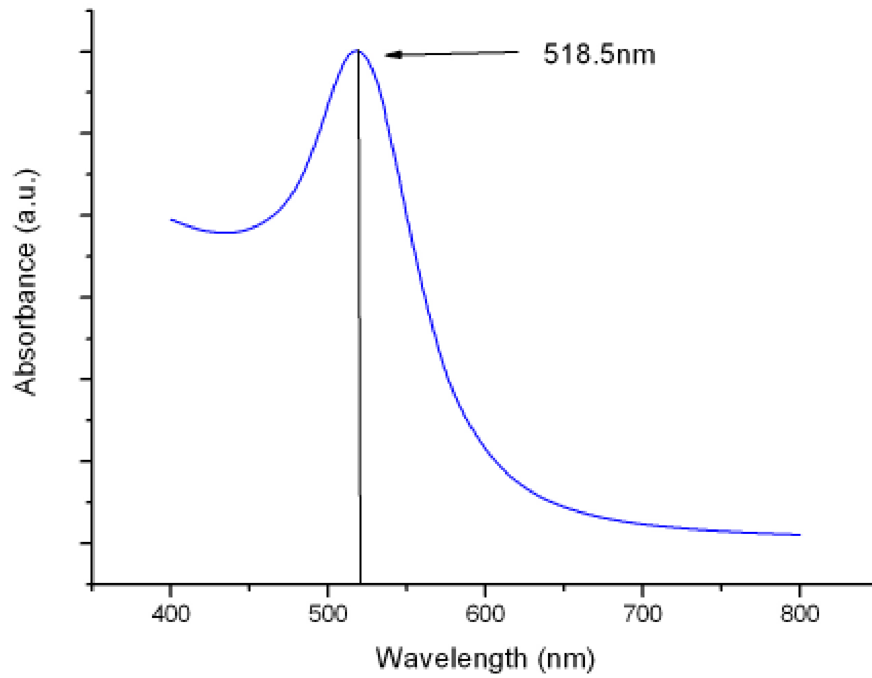

Figure 4-21. Absorption of gold nanoparticles dissolve in DI water measured by UV-Visible.

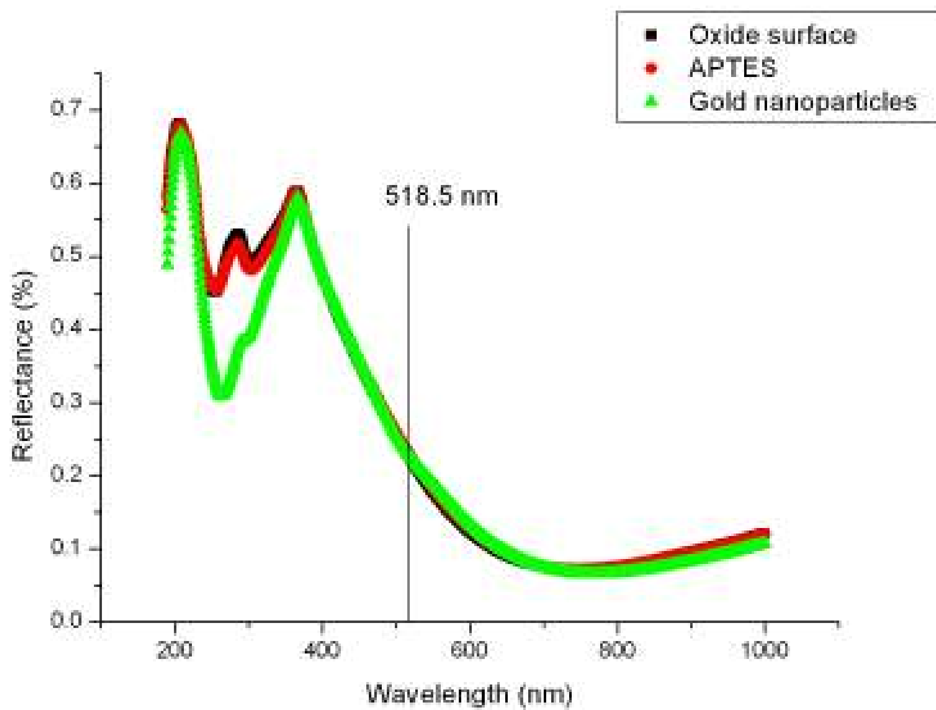

Figure 4-22. Reflection data of different surface by N&K measurement after each immobilization step.

Combine with absorption and SPR happened in the interface, these two reasons lead to small photo current to dark current ratio. We can easily improve the detector sensitivity by change incident light wavelength. If we replace the halogen lamp with 520nm laser diode, we can eliminate wavelength that non-absorbed by gold nanoparticles. In Figure 4-23, the dotted area is 520nm wavelength light that can be absorbed by gold nanoparticles, the white area is the incident light in visible range wavelenth. Dotted area divided by white area is the change in photo current to dark current ratio. Thus the sensitivity can be significantly improved then.

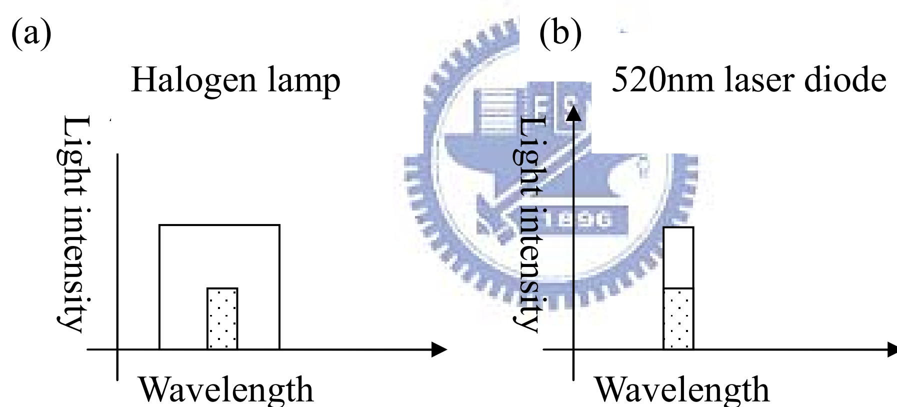

Figure 4-23. The model about how to improvement the sensitivity for gold nanoparticles detection. The dotted area is around 520nm wavelength, the white area is the incident light of (a) Halogen lamp, (b) 520nm laser diode.

Based on the strong chemical-bonding between gold and thiol, many molecules can be binding with gold nanoparticles, thus the gold nanoparticles immobilization on MSM-PD cab be used as a biosensor. The application can be used to detect lots bio-molecules when bio-molecules which satisfy the

requirements below:

1. The bio-molecules can't absorb 520nm wavelength light.

2. The bio-molecules contains thiol group.

If the molecules can absorb 520nm wavelength, thus we can't quantitatively analyze the sample. This method is dependent on gold nanoparticles absorbance at 520nm light, thus we don't know what the number of light is absorbed by gold nanoparticles. Besides, the molecules need to have thiol group, then it can bind onto gold nanoparticles by thiol-gold covalent bonding. There are various molecules in the sample and we can keep the molecules by thiol-gold bonding, if the molecules don't have thiol group then it will be removed after wash the sample.

Chapter 5: Conclusions

The Metal-Semiconductor-Metal photodetectors have been successfully developed for optical biosensor applications. The fabrication process of this device is simple, fast, and most important, the device is very cheap. We add a silicon oxide layer onto the MSM-PD unlike conventional devices. This silicon oxide layer has three main purposes: 1. Anti-reflection layer, 2. Immobilization surface, and 3. Passivation layer.

Active area of MSM-PD was defined by electron beam lithography and fabricated using standard semiconductor process. Combining reaction chamber made of PDMS, the MSM-PD as an on-chip biosensor for luminescence detection applications has been proposed. The calibration line with the minimal detection limit (MDL) is 4.9ng in 100uL PDMS reaction chamber. A gold nanoparticles detecting method is also demonstrated. These two applications are based on different mechanism. In luminescence application, the mechanism is based on the absorbance of luminescent emission light. In gold nanoparticles detection, the mechanism is based on gold nanoparticles absorbance at 520nm wavelength light. As we know biotin, streptavidin and gold nanoparticles can bind with many bio-molecules, thus these molecules, such as protein, DNA etc can be detected. This method can detect various bio-molecules. Most importantly, the system is portable and very low cost.